

Review

# Spectral Radiation Characteristic Measurements of Absorption and Scattering Semitransparent Materials—A Review

Meng Liu <sup>1</sup>, Shenghua Du <sup>1,2</sup>, Qing Ai <sup>1,\*</sup> , Jiaming Gong <sup>1,3,\*</sup> and Yong Shuai <sup>1</sup>

<sup>1</sup> Key Laboratory of Aerospace Thermophysics of MIT, School of Energy Science and Engineering, Harbin Institute of Technology, Harbin 150001, China

<sup>2</sup> Hebei Province Low-Carbon and Clean Building Technology Innovation Center, Yanshan University, Qinhuangdao 066004, China

<sup>3</sup> Institute of Industrial Science, The University of Tokyo, Tokyo 153-8505, Japan

\* Correspondence: hitaiqing@hit.edu.cn (Q.A.); jiaming@iis.u-tokyo.ac.jp (J.G.)

**Abstract:** The obtainment of spectral radiation characteristics of semitransparent materials mainly includes the use of a theoretical method or experimental method. As the experimental method can better characterize the real radiation transmission results inside the material, it is generally considered more reliable and used as the basis for the verification of theoretical results. In this paper, the absorbing and scattering semitransparent materials are taken as the analysis object to illustrate the research status and future development direction in the field of measurement and identification of spectral radiation characteristics. According to the physical quantities measured and the temperature range, research status is discussed for the spectral radiation characteristic measurements of absorbing and scattering semitransparent materials, which specifically involves the measurement principle, measuring system, measuring physical quantity, identification model and application range. This research will have guiding significance for the following research directions in the field of the acquisition of spectral radiation characteristic parameters of other new materials in the future.

**Keywords:** absorbing and scattering semitransparent materials; spectral radiation characteristics; transmission/reflection spectra; emission method; parameter identification



**Citation:** Liu, M.; Du, S.; Ai, Q.; Gong, J.; Shuai, Y. Spectral Radiation Characteristic Measurements of Absorption and Scattering Semitransparent Materials—A Review. *Energies* **2022**, *15*, 9013. <https://doi.org/10.3390/en15239013>

Academic Editor: Alessandro Cannavale

Received: 1 November 2022

Accepted: 25 November 2022

Published: 28 November 2022

**Publisher's Note:** MDPI stays neutral with regard to jurisdictional claims in published maps and institutional affiliations.



**Copyright:** © 2022 by the authors. Licensee MDPI, Basel, Switzerland. This article is an open access article distributed under the terms and conditions of the Creative Commons Attribution (CC BY) license (<https://creativecommons.org/licenses/by/4.0/>).

## 1. Introduction

With the development of aerospace, energy and chemical fields, the demand for material performance is higher, especially in extreme environments. Considering that radiation heat transfer plays an important role in the whole process of heat transfer in these application fields, it is of great significance to accurately obtain the spectral radiation characteristics of materials. As absorbing and scattering semitransparent materials exhibit outstanding radiation characteristics compared to traditional solid materials, they are increasingly used in corresponding areas, including solar thermal utilization [1–5], space thermal protection [6], photoanode substrate for solar cells [7] and so on. Absorbing and scattering semitransparent materials mainly include porous foams, nano-ceramic materials, thermal barrier coatings and so on.

Up to now, there are two main methods to obtain the spectral radiation characteristics of absorbing and scattering semitransparent materials. One is the theoretical method [8–11], which simulates the radiation transmission process based on the micro/nano structure obtained from numerical modeling [9,12,13] or real structure scanning [14], and describes its spectral radiation characteristics according to the statistical results. The other is the experimental method, which measures the apparent spectral radiation characteristics based on real micro/nano structural samples and inverts the basic spectral radiation characteristic parameters based on an identification program. In the theoretical simulation research, it is often necessary to simplify the material structure and adopt some assumptions for

the convenience of calculation. In addition, due to the complexity of structure for this kind of material, the numerical method has a huge amount of calculation. By contrast, the experimental method takes less time and has higher reliability as it reflects the real radiation transfer process in materials, which can be used as a benchmark for the verification of theoretical results. Therefore, experimental means have important research significance and are also the direction of researchers' unremitting efforts.

Throughout the development of measurement methods for spectral radiation properties of materials, the main methods have included transmission, reflection and emission methods. The transmission method is based on the definition of transmission ratio, which is the ratio between the detected signal intensity in a certain direction after the light source penetrates the sample and the detected signal intensity when the light source is not attenuated by the sample. The reflection method is based on the definition of reflection ratio, that is, the ratio of the signal intensity detected in a certain direction after the light source is reflected by the sample and the signal intensity detected in that direction after the light source is reflected by the standard sheet. The emission method is based on the definition of emissivity, which is the ratio between the radiation intensity of a sample at a certain temperature and the radiation intensity of a blackbody at the same temperature, while the normal emittance is the main measurement quantity in published research. In transmission and reflection methods, the incident radiation comes from the external light source, which can be distinguished from the emitted signal of the sample after the modulation of a chopper or interferometer. However, in the emission method, the detected radiation intensity is from the sample itself without modulation, which is unable to be distinguished from the stray radiation signals around, so it is necessary to eliminate the stray radiation signal when dealing with the actual measurement results. For opaque solid materials, only environmental radiation signal interference needs to be removed from measurement results, but for semitransparent materials the radiation signal interference of the heating source also needs to be shielded, which is more complicated to deal with.

For the last two decades, international institutions conducting research on the radiation characteristic measurements of absorbing and scattering semitransparent materials mainly include the National Scientific Research Center of France, Institute for High Temperatures of the Russian Academy of Sciences, Bavaria Applied Energy Research Center in Germany, etc., while in China, such research institutions mainly include Shanghai Jiao Tong University, North China Electric Power University, Harbin Institute of Technology, etc. Early research in this field included not only the establishment of experimental systems and corresponding radiation characteristic measurements, but also the establishment of an identification model for basic radiation characteristic parameters. However, later research mainly focuses on carrying out radiation characteristic measurements based on existing experimental systems, so as to verify the reliability of theoretical simulation results.

According to the depth of authors' understanding, this article describes the methods adopted by domestic and foreign researchers in the research field of spectral radiation characteristic measurements for absorbing and scattering semitransparent materials from multiple angles comprehensively. The corresponding results obtained from normal temperature to high temperature, from hemisphere to direction characteristics and from the measuring system to the identification model, and the advantages and disadvantages of these measuring systems are discussed in detail, which points the way for further development of this field.

## 2. Measuring Systems for Spectral Radiation Characteristics at Room Temperature

The spectral radiation characteristic measurements at room temperature mainly focus on obtaining bi-directional transmission/reflection spectra and direction-hemispherical transmission/reflection spectra. The measurement system is either based on the laser modulated by a chopper as the light source and the lock-in amplifier and photodetector as the detection device, or based on the continuous light source modulated by interferometer and an FTIR spectrometer as the detection device. Due to the single wavelength of the

laser, the laser chopper modulation system can only obtain the experimental data under several single wavelengths, and is susceptible to the interference of external radiation signals. In contrast, an FTIR spectrometer has the advantages of continuous spectrum, stable system and strong signal-to-noise ratio, so it has been widely used in spectral signal measurement. In addition, the thickness of the sample used in measurements should be chosen carefully as it cannot represent the real structure if the sample thickness is too thin because of insufficient cells. According to numerical research [15], the sample thickness should exceed 2.4 times of the equivalent cell diameter when the porosity floating rate is 0.05, and 3.5 times when the change rate is 0.02.

### 2.1. Directional Transmission/Reflection Spectrum Measurement at Room Temperature

At the beginning of design, an FTIR spectrometer was mainly used for component detection in the chemical and pharmaceutical fields, therefore, the internal optical path was designed as a convergent beam to enhance the detection signal intensity. Gradually, along with the development of the radiation measurement field, the FTIR spectrometer was introduced to obtain the radiation spectrum curves of materials, but its internal light path was preserved, whose convergence property would have certain influence on the detection results. However, the researchers generally assume that the incident beam inside the FTIR spectrometer is normal. In 1996 [16], researchers from the University of California measured the normal transmittance and normal reflectance spectra of aerogel materials by the internal optical light path of an FTIR spectrometer in the wavelength range of 2.5~25  $\mu\text{m}$ , which ignored the scattering characteristics of the sample. In 2016 [17], Zhang et al. from Georgia Institute of Technology obtained the normal transmittance spectra of ceramic  $\text{Al}_2\text{O}_3$ ,  $\text{AlN}$  and  $\text{Si}_3\text{N}_4$  by the internal optical path of an FTIR spectrometer directly. In 2011 [18] and 2013 [19], Wei et al. from North China Electric Power University measured the transmittance spectra of aerogel and its composite insulation material in the mid-infrared band by the internal optical path of an FTIR spectrometer, which regarded the measured results as normal transmittance spectra that could be used to calculate the extinction coefficient of materials directly according to Beer's law. Then, in 2017 [20], this research group measured the transmittance spectra of  $\text{Al}_2\text{O}_3$  ceramics and  $\text{ZrO}_2$  ceramics by the internal optical path of an FTIR spectrometer in the wavelength range of 2.5~25  $\mu\text{m}$ , while the normal incidence assumption was also adopted.

With the development of the spectral radiometry field, the convergence characteristics in the internal optical path of an FTIR spectrometer was gradually realized by some researchers. In 2014 [21], researchers in KIT measured the spectral transmittance and diffuse reflectance of alumina ceramics, mullite,  $\text{SiC}$  oxide and cordierite by the internal optical path of an FTIR spectrometer combined with the diffuse reflectance accessory (PIK-UPIR) in the wavelength range of 2.5~27  $\mu\text{m}$ , which pointed out that the convergent spot diameter of the incident beam was 8 mm in the sample compartment, but the influence of the convergent incident beam on the final measurement results was not further analyzed. In 2022 [22], researchers at the Harbin Institute of Technology analyzed the applicability of the internal optical path of an FTIR spectrometer for transmission measurements of absorbing and scattering media, and gave a modified formula for the detected transmittance.

The convergence property of the internal light path of an FTIR spectrometer increased the complexity of data processing for spectral radiation measurements, and there were certain deviations in measurement results under normal assumption. Based on this, Bailis [23] established the measurement platform for bi-directional transmission/reflection spectra based on the external light path of an FTIR spectrometer in 1999, as shown in Figure 1. This experimental system adopted the nearly parallel beam drawn out from an FTIR spectrometer with the divergent angle of  $0.87^\circ$  and set the sample and detector on two rotating platforms, respectively, by which the bi-directional transmission/reflection spectra of carbon foams were measured in the wavelength range of 2~15  $\mu\text{m}$ . Then, in 2002 and 2004, the experimental setup shown in Figure 1 was used to measure the bi-directional

transmission/reflection spectra of polyurethane foams [24,25], fibrous materials [25] and quartz materials containing bubbles [26].

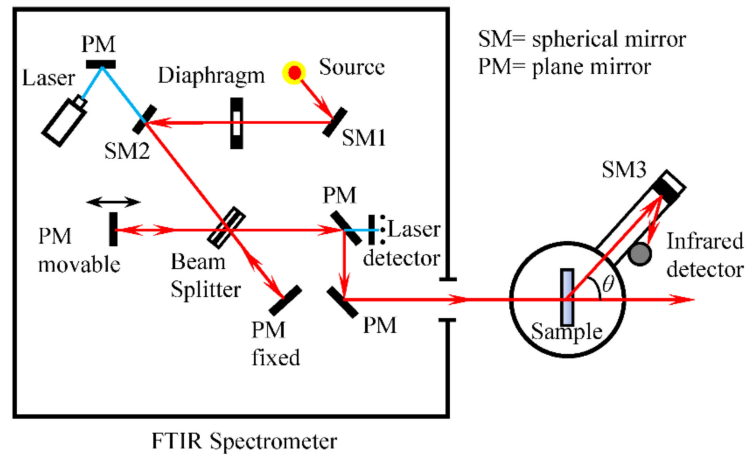


**Figure 1.** Experimental system of bi-directional transmission/reflection spectra based on the external optical path of an FTIR spectrometer [23].

By contrast, lasers can only emit light of a single wavelength, which needs to be modulated by a chopper and detected by lock-in amplifier and photodetector. In 2006 [27], the Laboratory of Molecular and Macroscopic Energy of the Central Institute of Technology measured the bi-directional transmission/reflection signals of mullite with the experimental system shown in Figure 2. This experimental system took the He-Ne laser at 632.8 nm as the light source with a diameter of 8 mm by beam expansion, modulated by a chopper and detected by lock-in amplifier and photodetector, while the directions of sample and detection device were controlled by the rotating mechanism. In 2013 [28], Zhang et al. from the Harbin Institute of Technology measured the bi-directional reflection intensity distribution (BRDF) of copper foams by the experimental system shown in Figure 3, which took the He-Ne laser at 660 nm after beam expansion as the light source. The reliability of this system was verified by a single silicon wafer.

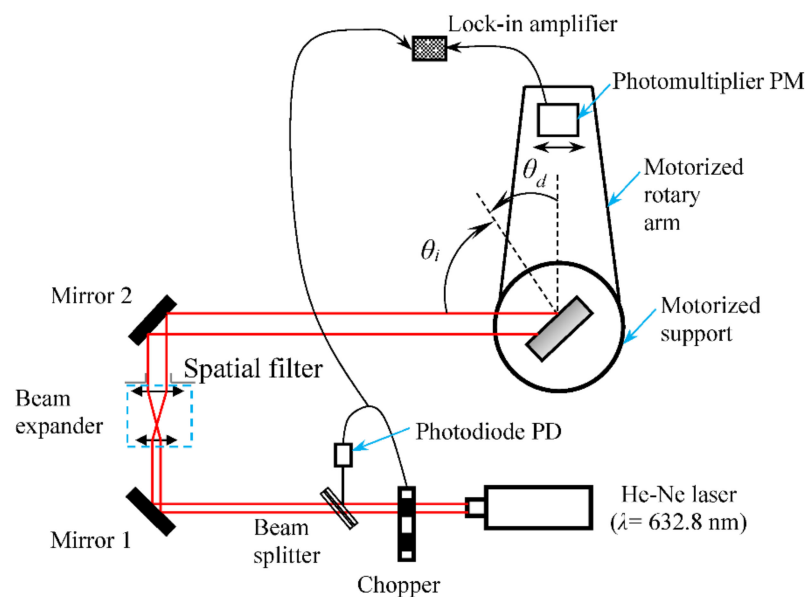


**Figure 2.** Bi-directional transmission/reflection measurement system based on the laser chopper system [27].

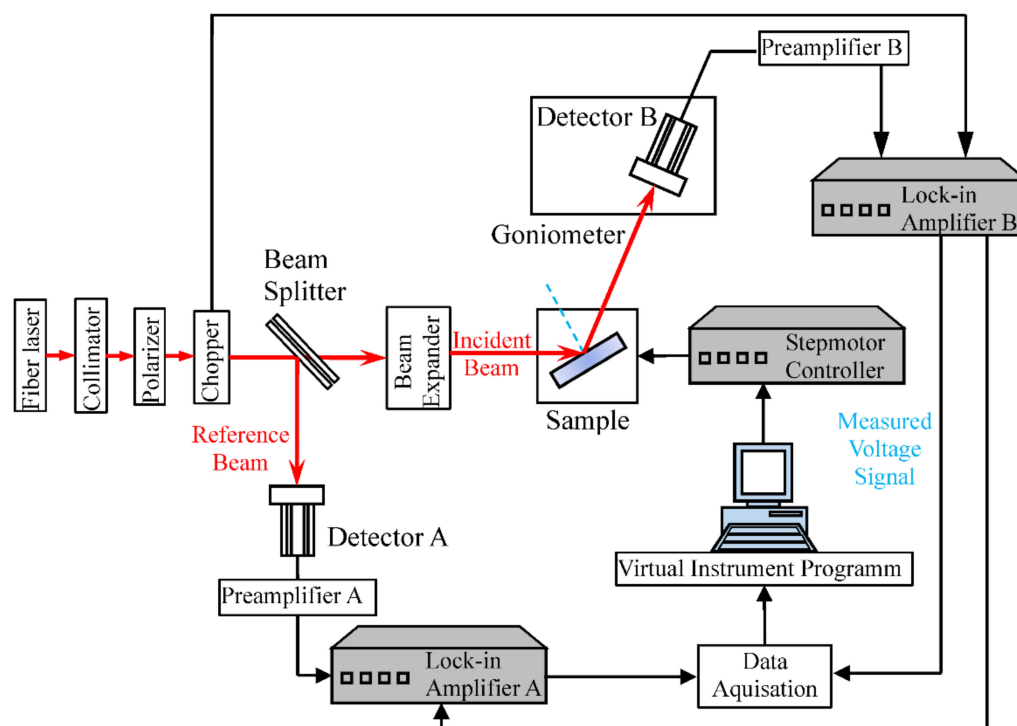


**Figure 3.** Schematic diagram of the BRDF measurement system [28].

The grating monochromator separates the composite beam entering its incident slit into monochromatic light in a wide spectral range by the diffraction effect of grating, and can be automatically scanned by computer control, which is equivalent to a light source system integrated with multiple lasers, and has been widely used. Considering that the light emitted by the grating monochromator is not modulated, it is necessary to equip the chopper and lock-in amplifier in the actual construction of the measurement system. In 2002 [29], the Laboratory of Applied Theoretical Mechanics and Energy of the Advanced Institute of Engineering Science and Technology of Nanci built a bi-directional transmission/reflection spectra measurement system similar to Figure 1 based on the monochromator, as shown in Figure 4, which adopted the double rotary table mechanism to control the position of the sample and the detection device, and was applied to fiber materials. In 2011 [30], Coray et al. from the Solar Technology Laboratory of Paul Scherrer Institute in Switzerland proposed the experimental system shown in Figure 5 to measure the bi-directional transmission/reflection spectra of semitransparent media in the wavelength range of 0.3–4  $\mu\text{m}$ , which took the grating monochromator as the light source and added a rotating device to the detection system to realize multi-angle measurement, and then Marti [31] et al. used this spectroscopic goniometry system to measure the radiative property of SiC particle suspensions. This system was improved in 2016 [32] with the wavelength range from 0.3 to 2.5  $\mu\text{m}$ . In addition, the School of Mechanical Engineering in the University of Minnesota [33,34] built a bi-directional transmission measurement system based on the grating monochromator as the light source, as shown in Figure 6, while the irises on both sides of the sample could be used to limit the incoming and outgoing beam diameters. The measurement object of this study was cerium dioxide ceramic material, as the measurement wavelength range was 0.35–2  $\mu\text{m}$ , the incident radiation cone angle was about  $4.2^\circ \pm 0.3^\circ$  and the outgoing radiation cone angle was about  $6^\circ \pm 0.5^\circ$ , however, the influence of these cone angles on the measurement results was not analyzed in the subsequent study.

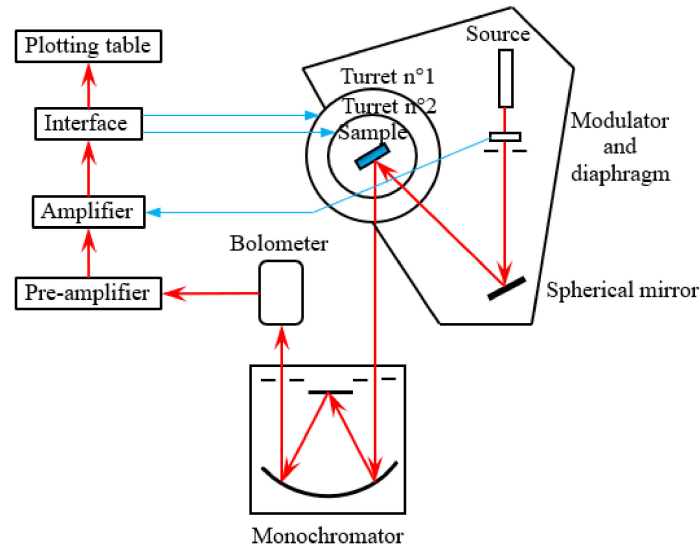


**Figure 4.** Bi-directional transmission/reflection spectra measurement system based on the grating monochromator [29].

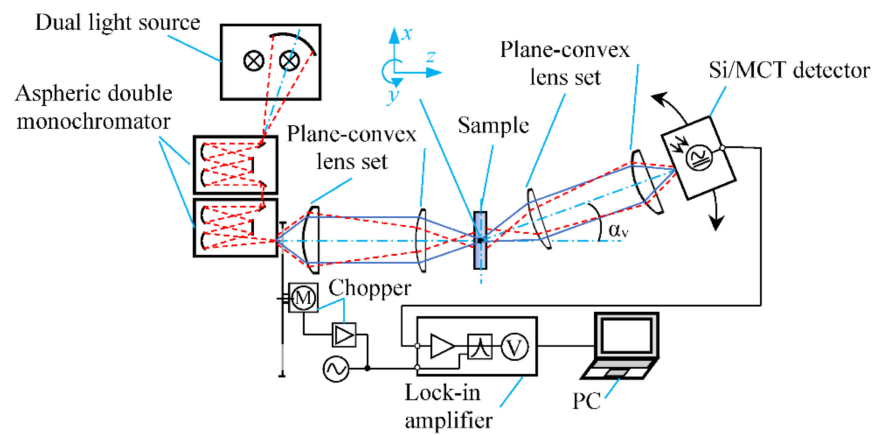


**Figure 5.** A spectral angle measuring system [30] to determine the thermal radiation characteristics of participation media.

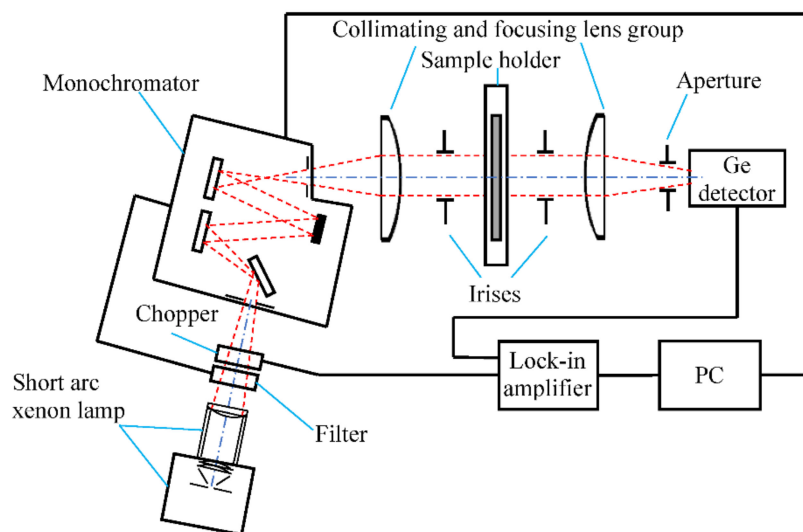


**Figure 6.** Schematic diagram of the normal-normal transmission measurement system [33,34].

## 2.2. Hemispherical Transmission/Reflection Spectrum Measurement System at Room Temperature

Considering that absorbing and scattering semitransparent materials usually have strong scattering characteristics, it is difficult to detect the radiation signal in some directions as it is too weak, although the measurements of directional spectral radiation characteristics can supply more information. Therefore, the acquisition of direction-hemispherical transmission/reflection spectra is also a necessary means to study the radiation characteristic parameters of such materials.

The direction-hemispherical transmission/reflection spectra measurements can be performed directly by the internal optical path of an FTIR spectrometer when the integrating sphere is attached. In 2004 [35], Zhao et al. measured the direction-hemispherical transmission/reflection spectra of FeCrAlY metal foam by the internal optical path of an FTIR spectrometer equipped with the copper hemisphere in the wavelength range of 2.5–50  $\mu\text{m}$ , but the parallelism of the incident beam was not specified, for which we suspect they adopted the assumption of normal incidence, as the attenuation coefficient of the sample was calculated according to Beer's law in the data processing. In 2013 [36], Zhao et al. measured the direction-hemispherical transmission/reflection spectra of thermal barrier coatings by the internal optical path of an FTIR spectrometer combined with integrating sphere accessory in the wavelength range of 0.25–25  $\mu\text{m}$ , which assumed normal incidence as the incident angle of light source less than  $2^\circ$ , and the average of three measurement results was calculated for each sample. In 2008 [37], researchers from NASA measured the normal-hemispherical transmission/reflection spectra of YSZ thermal barrier coating using the internal optical path of an FTIR spectrometer combined with the integrating sphere in the wavelength range of 0.8–25  $\mu\text{m}$  with the assumption of normal incidence. In 2012 [38], Baillis et al. measured the normal-hemispherical transmission/reflection spectra of Al-NiP foam based on the internal optical path of an FTIR spectrometer equipped with a gold-coated integrating sphere in the wavelength range of 2–20  $\mu\text{m}$  under the assumption of normal incidence. In 2014 [39,40], researchers from Louisiana State University measured the direction-hemispherical transmission/reflection spectra of 8YSZ thermal barrier coating and plasma-sprayed BaZrO<sub>3</sub> coating using the internal optical path of an FTIR spectrometer combined with the integrating sphere under the assumption of normal incidence. In 2016 [17], Zhang et al. measured the direction-hemispherical transmission-reflection spectra of Al<sub>2</sub>O<sub>3</sub> ceramics, AlN ceramics and Si<sub>3</sub>N<sub>4</sub> ceramics using the internal optical path of an FTIR spectrometer equipped with a gold-coated integrating sphere in the wavelength range of 1.67–15.6  $\mu\text{m}$ .

There are also research institutions carrying out direction-hemispherical transmission/reflection spectra measurements based on the integrating sphere accessory arranged outside an FTIR spectrometer. In 1997 [41] and 1998 [42], the Bavarian Applied Energy Research Center and the University of Wurzburg cooperated to measure the direction-hemispherical transmission/reflection spectra of the powder using the external optical path of an FTIR spectrometer combined with the integrating sphere (coated gold/BaSO<sub>4</sub>) in the wavelength ranges of 1.4–20  $\mu\text{m}$  and 0.3–2.5  $\mu\text{m}$ , respectively, however, the parallelism of the incident beam is not pointed out. In 1999 [43], Manara et al. measured the direction-hemispherical transmission/reflection spectra of sintered Al<sub>2</sub>O<sub>3</sub> ceramics by the external optical path of an FTIR spectrometer combined with the integrating sphere (BaSO<sub>4</sub>) in the wavelength range of 0.7–2.5  $\mu\text{m}$ , but the parallelism of the incident beam was still not considered in this study. On the basis of the bi-directional transmission/reflection spectrum measurement system shown in Figure 1, Baillis et al. added the measurement system for direction-hemispherical transmission/reflection spectra of carbon foams in 2000 [44], in the wavelength range of 0.1–2.1  $\mu\text{m}$ , as shown in Figure 7. In 2002 [24,25,45], this research group used this system to measure the direction-hemispherical transmission/reflection spectra of polyurethane foam and fiber materials, and assumed that the incidence of light source was parallel normally. In 2007 [46], this research group cooperated with the Institute for High Temperatures of the Russian Academy of Sciences to measure the direction-hemispherical transmission/reflection spectra of zirconia ceramics

by an FTIR spectrometer combined with integrating sphere in the wavelength range of 2.5~9  $\mu\text{m}$ . In 2019 [47], this research group measured the hemispherical transmittance and hemispherical reflectance of expanded polystyrene foams with opacifying particles. In addition, the FTIR spectrometer combined with integrating sphere was used to measure the direction-hemispherical transmission/reflection ratio of low-emitting transparent coatings based on tin-doped indium oxide [48] and aluminum-doped zinc oxide [49], the EB-PVD YSZ thermal barrier coating [50], the 4-layered ITO-coating [51], the 11-layered AZO-coating [51] and the polymer-based pigmented coatings on substrates [52] under the condition of normal incidence in the wavelength range of 0.25~35  $\mu\text{m}$ , and the extruded polystyrene foam, polyurethane foam [53] and opacified extruded polystyrene foam [54] in the wavelength range of 1.4~35  $\mu\text{m}$ . There were also researchers adopting the spectrophotometer and integrating sphere to measure hemispherical transmittance/reflectance, for example, Zhao [55] et al. measured hemispherical transmittance/reflectance of silica aerogels in the wavelength range of 0.25~2.5  $\mu\text{m}$  with the integrating sphere of polytetrafluoroethylene (PTFE) coating, Li [56] et al. measured the specular reflectivity and total reflectivity by a UV-Vis-NIR spectrophotometer and its integrating sphere accessory in the wavelength range of 0.25~2.5  $\mu\text{m}$ , while Elisa [57–59] et al. measured the hemispherical reflectance of novel ice-templating porous  $\text{ZrB}_2$  ultra-high temperature ceramics (UHTCs),  $\text{TaB}_2$  dense ceramics and  $\text{TiB}_2$  ceramics using a double-beam spectrophotometer equipped with a Spectralon-coated integrating sphere for the 0.25~2.5  $\mu\text{m}$  wavelength region and an FTIR spectrometer equipped with a gold-coated integrating sphere for the 2.5~15  $\mu\text{m}$  wavelength region, and Audrey [60,61] et al. measured the hemispherical reflectance in the UV to mid-IR range (0.25~2.5  $\mu\text{m}$ ) for  $\text{TiAlN}_x/\text{TiAlN}_y/\text{Al}_2\text{O}_3$  tandem solar selective absorber coatings and  $\text{TiAlC}/\text{TiAlCN}/\text{TiAlSiCN}/\text{TiAlSiCO}/\text{TiAlSiO}$  coating.

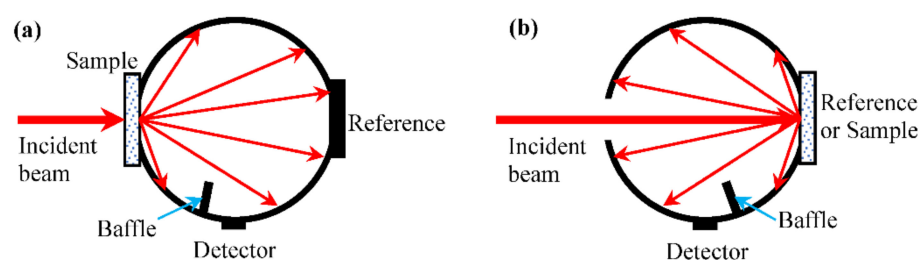


**Figure 7.** Measurement system [44] diagram of (a) direction-hemispherical transmittance and (b) direction-hemispherical reflectance.

Although the light emitted by the grating monochromator is of multiple independent wavelengths, it can realize automatic scanning in a certain wide band range, so it can also be used to build the experimental bench for measuring the direction-hemispherical spectral radiation characteristics. In 2013 [33], the School of Mechanical Engineering in the University of Minnesota, in cooperation with the Institute for High Temperatures of the Russian Academy of Sciences, built the direction-hemispherical transmission measurement system based on a grating monochromator, as shown in Figure 8, and used it to measure the direction-hemispherical transmission spectra of cerium dioxide ceramic materials in the wavelength range of 0.35~2  $\mu\text{m}$ . In 2016 [32], Coray et al. built a direction-hemispherical transmission/reflection spectra measurement system based on a grating monochromator, and obtained the spectral reflection signals of silver-coated glass and the spectral transmission signals of thin film materials, such as ETFE, in the wavelength range of 0.3~2.5  $\mu\text{m}$  under the assumption of uniform distribution of incident radiation with incident solid angle.

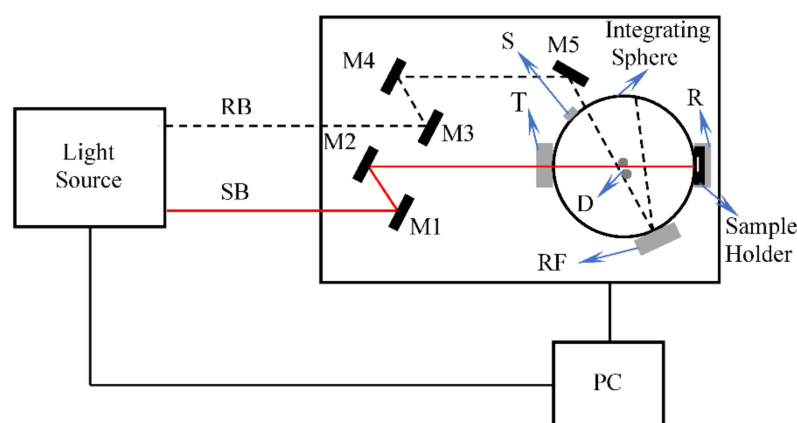


**Figure 8.** Normal-hemispherical transmission measurement system [33].

Through the above analysis, it can be found that the laser and monochromator need to be modulated by a chopper and lock-in amplifier device when they are used as independent light sources before carrying out corresponding spectral radiation characteristic measurements. By contrast, an FTIR spectrometer is more perfect and reliable, so most researchers choose to perform spectral radiation characteristic measurements based on an FTIR spectrometer in practical applications. For the experimental research on spectral radiation characteristic measurements based on an FTIR spectrometer, researchers from the National Center of scientific research in France and Bavarian Applied Energy Research Center in Germany mostly adopted the external optical path of a spectrometer, among them, the French research institute realized the bi-directional transmission/reflection measurements by constructing a double rotary mechanism to fix the sample and the detector and pointed out the divergence angle of the incident beam, which were ignored by other research institutes who assumed normal incidence. In addition to these, other research institutes mostly performed measurements on the internal optical path of an FTIR spectrometer, either directly measuring the normal-normal transmission/reflection signals, or obtaining the normal-hemispherical transmission/reflection signals based on the integrating sphere accessory, but this research all adopted the assumption of normal incidence and ignored the convergent characteristics of the internal optical path, which had an impact on the measured results. However, the influence of this factor was not analyzed in these studies. Moreover, the radiation properties of absorbing and scattering semitransparent materials are mostly measured at room temperature based on this kind of system, and the influence of temperature is rarely involved.

### 3. Measuring System for Spectral Radiation Characteristics at High Temperature

Considering that the scattering characteristics of absorbing and scattering semitransparent materials is stronger, and the directional spectral radiation signals are weak and difficult to detect, and at the same time their own emission radiation will further interference the detection signal under the condition of high temperatures, the measurements of bi-directional transmission/reflection spectra for this kind of material are generally carried out at room temperature and rarely involved high temperatures. In addition, as the integrating sphere accessory cannot withstand high temperature environments, the direction-hemispherical spectral radiation characteristics are also performed at room temperature in most research. Based on this, the experimental research on spectral radiation characteristics of absorbing and scattering semitransparent materials under high temperatures mostly adopt the emission method.

#### 3.1. Transmission/Reflection Spectrum Measurement System at High Temperature

Among the published studies, the high temperature normal-hemispherical reflectance measurement system was proposed in 2001 [62] by the Institute for High Temperatures of the Russian Academy of Sciences, as shown in Figure 9. The system used a  $10.6 \mu\text{m}$   $\text{CO}_2$

laser as the radiation heating source and performed real-time temperature measurements through a radiation pyrometer in the temperature range from room temperature to 3200 K. At the same time, the normal-hemispherical reflectance spectra of zirconia ceramic materials were obtained using the laser at 0.488  $\mu\text{m}$ , 0.6328  $\mu\text{m}$ , 1.15  $\mu\text{m}$  and 1.39  $\mu\text{m}$  wavelengths as the incident light sources. However, the material used for the integrating sphere was not explained and the temperature field inside the integrating sphere was not analyzed specifically. Then, Zhang [63] et al. at the Harbin Institute of Technology built an integrating-sphere reflectometry to measure the spectral reflectivity, which could be used to calculate the spectral emissivity based on Kirchhoff's Law; the schematic diagram is drawn in Figure 10. In addition, White [64] from the AmU Research Center of NASA established the experimental system to measure normal transmission spectra based on solar radiation in 2010, as shown in Figure 11, which took a fiber optic spectrometer as the detection device in the visible and near-infrared bands. The sample was porous fiber material in this study, but the measurement temperature was not indicated.

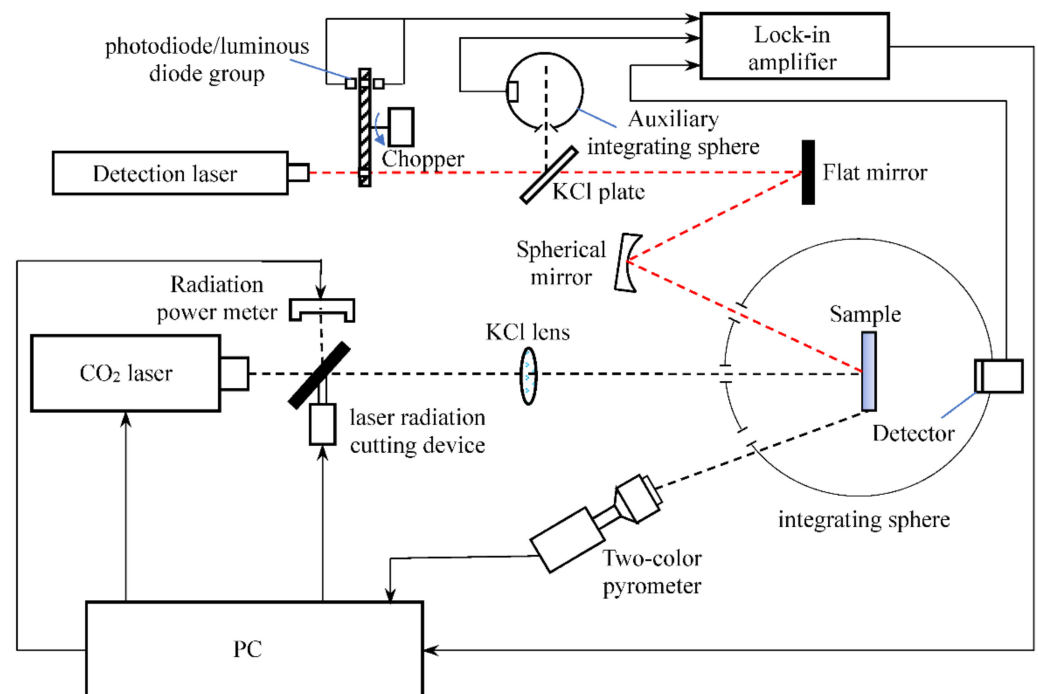


Figure 9. Measurement system of normal-hemispherical reflectance under high temperatures [62].

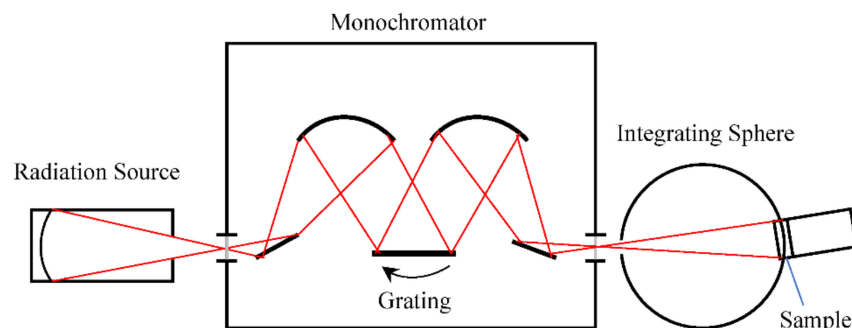
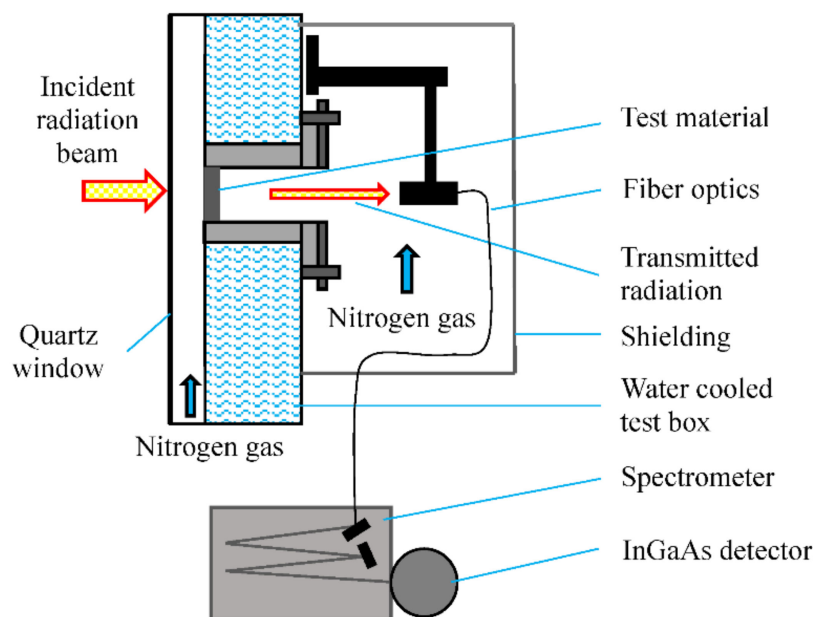


Figure 10. Schematic diagram of the optical system [63].



**Figure 11.** Schematic diagram of transmission spectrum measuring system based on solar radiation [64].

### 3.2. Emission Spectrum Measurement System at High Temperature

Different from the transmission/reflection measurement, the emission measurement cannot adopt external light source, as the sample itself is the radiation source. Since the measured signal cannot be modulated in advance, the source and influence of various stray radiation signals should be fully considered in the actual measurement results to obtain accurate emission signals of samples. Sample heating is a key part of emission measurement, and heating methods currently developed mainly include the following: electric heating, high-temperature furnace heating, laser heating, xenon lamp heating, flame heating [65] and so on. Considering the upper limit of temperature of electric heating is low, as it is affected by power, the flame heating may pollute the sample, as it needs to contact the sample, and the working temperature of furnace heating is also limited by the material of heating rod, by contrast, the radiation heating method based on laser or xenon lamp is the best choice for carrying out high temperature emission measurements of absorbing and scattering semitransparent materials because of wider temperature range, more exploitability, and cleaner heating environment.

Electric heating [66], as the most common heating method, usually places the sample in a cylindrical heating chamber and heats it on one side, as shown in Figure 12. Electric heating belongs to a contact heating mode based on heat conduction from the metal plate attached behind the sample, but the temperature is limited by the electric power. For the system shown in Figure 13a, the surface temperature of the sample could reach 770 °C and the entire system was set in the stainless-steel cavity with water cooling and internal blackening under the condition of atmosphere or vacuum. The system in Figure 13b is a similar contact electric heating system. Considering that this kind of heating method adopts one-sided heating, better thermal conductivity of the sample is usually needed, otherwise a large temperature gradient will be generated in the axial direction, which will affect the emission signal measurement of thermal insulation materials.

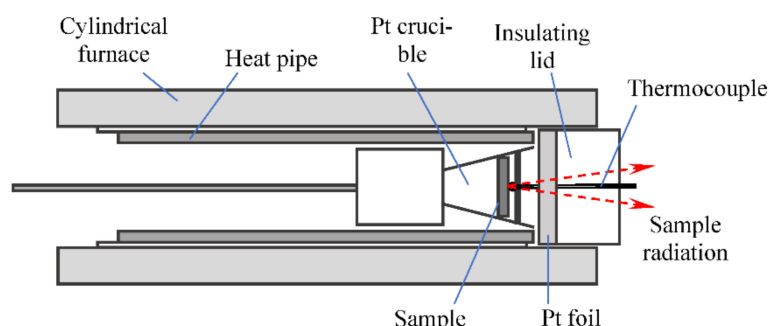
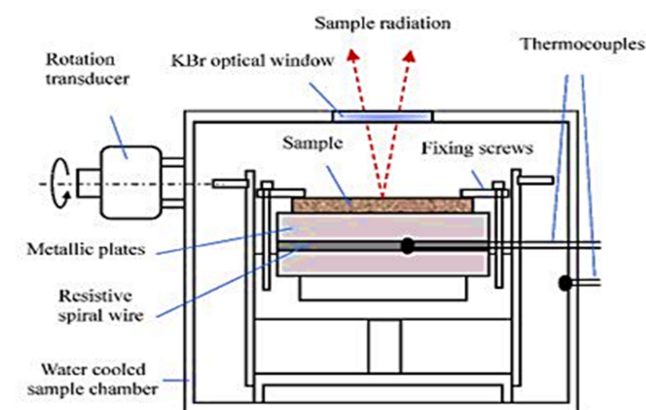
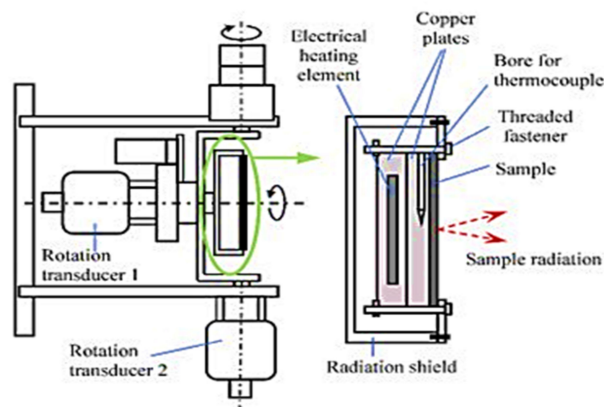


Figure 12. Electric heating device [66] with a cylindrical high-temperature furnace.



(a)



(b)

Figure 13. Contact electric heating device (a) del Pais Vasco Laboratory of University of Spain [67] and (b) Helmut-Schmidt University Laboratory, Germany [68].

As absorbing and scattering semitransparent materials are semitransparent media, the radiation signal of the heating element will interfere with measurement results. Based on this, the Korea Institute of Standards Science and Technology proposed the double substrate method from 2010 to 2013 [69–71], whose principle is shown in Figure 14. Two materials with different emissivity were used as substrates in the measurement, and the actual emissivity of the sample was solved through analyzing the relationship between the measured signal, the base signal and the signal of the sample to be measured. In this study, the sample was heated by thermal conduction of the substrate, while gold and black paint were used as the substrate materials, and the radiation signal was detected by an FTIR spectrometer in the wavelength range of 2.5–25  $\mu\text{m}$  up to 1200  $^{\circ}\text{C}$ . To ensure good contact between the sample and the substrate, the sample was polished in this study, including sapphire and  $\text{Al}_2\text{O}_3$  ceramics.

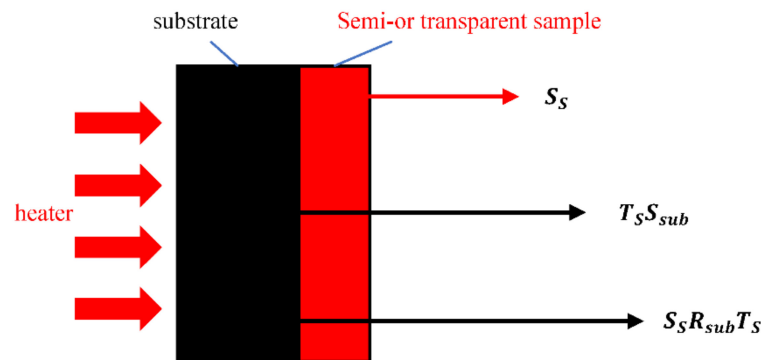


**Figure 14.** Schematic diagram of the double substrate method [69–71].

With the development of aerospace, energy and chemicals, the radiation characteristics of materials in extreme environments have attracted more and more attention. At the same time, it is crucial to accurately obtain the radiation characteristics of materials at high temperature as the radiation heat transfer occupies a large share in heat transfer under high-temperature conditions. Driven by demand, radiation heating methods are developed gradually, including high-temperature furnace heating, flame heating, laser heating, xenon lamp heating and so on, which have advantages of higher temperature upper limit and faster heating rate.

In the heating mode of high-temperature furnaces, the high-temperature furnace usually has a closed structure purchased commercially, while the upper limit of heating temperature is higher than that of electric heating, but there is still a certain upper limit of temperature restricted by heating elements. In addition, the emission measurement results will be interfered by the radiation signal emitted by the inner wall of the high-temperature furnace. In 2017 [72], the emissivity of ZrB<sub>2</sub>-SiC composite was measured by the China Academy of Engineering Physics based on the emissivity principle using an FTIR spectrometer in the wavelength range of 2.5–25  $\mu\text{m}$ , while the sample was heated by a high-temperature furnace and the temperature was measured by K-type thermocouple in the temperature range of 573–1173 K. On the basis of heating samples in a high-temperature furnace, the University of Central Florida [73] used the system shown in Figure 15 to carry out emissivity measurement. In this system, the sample was heated to isothermal in the high-temperature furnace and measured by the radiation protection tube inserted into the furnace, which is shown in Figure 16. The optical fiber head is placed in a fixed position in the sunshield cylinder in order to avoid the radiation from the high-temperature furnace wall, heating element and ambient gas into the optical fiber end. In addition, the space between the fiber cladding and the inner wall of the shade cylinder was filled with SiO<sub>2</sub> fibers for insulation, and the measurement time for each sample did not exceed 3 s, which can guarantee the shading cylinder would not be heated to a higher temperature and its emission radiation would not affect the emission measurement of the sample. Experiments in this study were operated on the YSZ thermal barrier coating with a thickness of 2 mm in the wavelength range of 0.4–1.08  $\mu\text{m}$  and temperature range of 673–1423 K by grating spectrometer. However, it was not stated whether and how much the insertion of the radiation protection tube would affect the sample temperature in the study. Then, Rydzek [74] et al. at the Bavarian Center for Applied Energy Research designed an emittance measurement apparatus to measure the angular dependent surface emittance of TiO<sub>2</sub>/Y<sub>2</sub>O<sub>3</sub> ceramics, copper and an alloy at temperatures up to 1673 K with the detection angle from 0° to 85°. This apparatus adopted a cylindrical tube furnace with a wrapped electric resistance heating wire to heat samples in a vacuum or gaseous atmosphere. Some other researchers manufactured their own high-temperature heating cavity, as shown in Figure 17, which took the SiC tube as the sample heating cavity in the National Defense University of Munich [75] (2013) to build the emissivity measurement system in the wavelength range of 0.6–15  $\mu\text{m}$  and the temperature range of 773–1623 K. It was concluded that the length of the SiC tube met the isothermal region length of the

tubular heater, and the measurement was carried out in atmosphere without encapsulated windows. The sample for measurement was a sintered SiC sample with a thickness of 5 mm and was mounted behind a conical water-cooled sample cooler to prevent the reflected radiation on the sample surface from being detected, as shown in Figure 18.

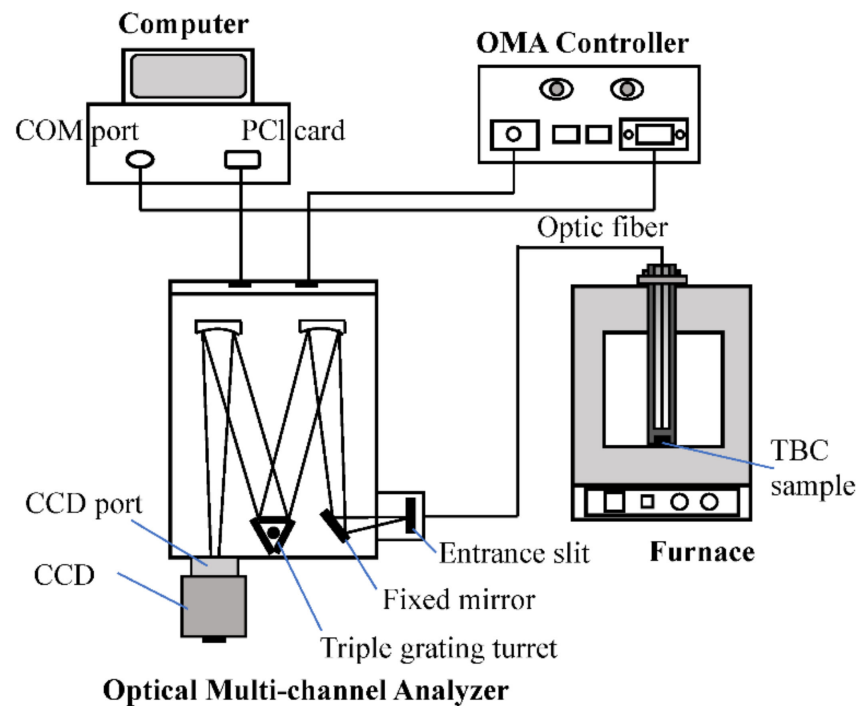


**Figure 15.** Schematic diagram of the system for emissivity measurement based on a high-temperature furnace [73].

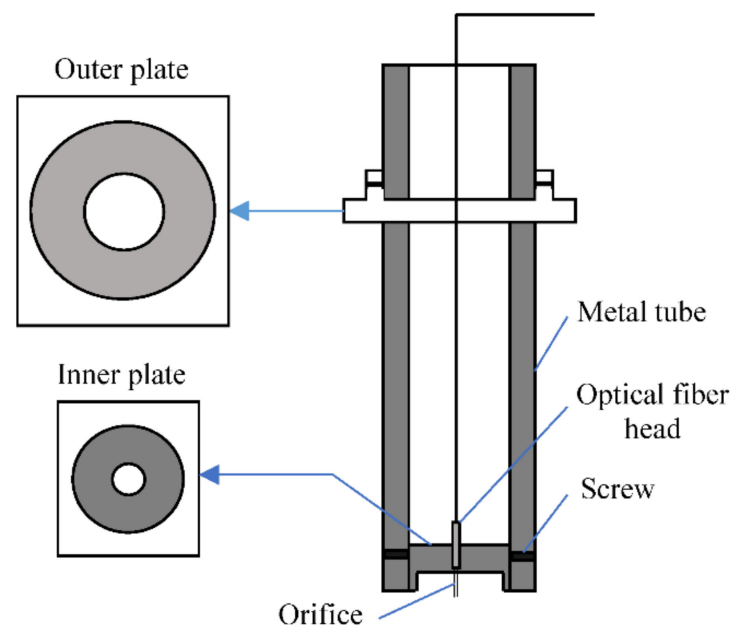


**Figure 16.** Design schematic diagram of a radiation shading cylinder [73].

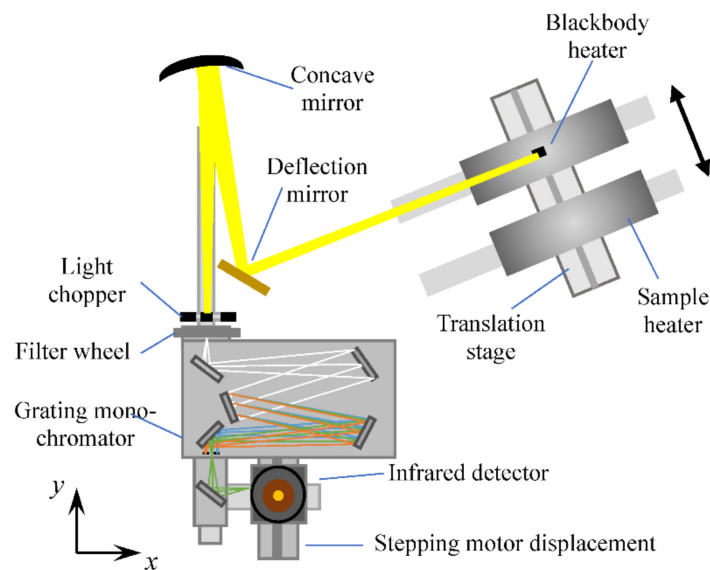


**Figure 17.** Schematic diagram of the device made by the SiC tube as the sample heating cavity [75].

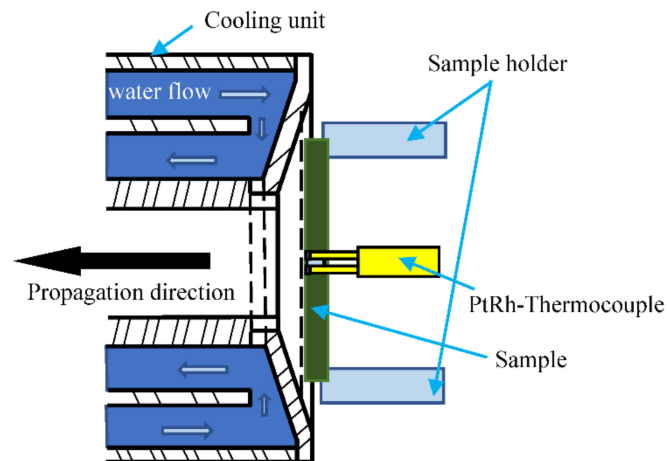


**Figure 18.** Schematic diagram of sample installation when the sample was heated by the SiC tube [75].

Compared to the heating method of a high-temperature furnace, flame heating has a higher upper temperature limit and faster heating rate, but it may cause pollution to the heated sample, and it is difficult to shield the radiation interference from the heating source for semitransparent materials. In 2014 [76], Wang from the Nanjing University of Science and Technology built the high-temperature normal emissivity measurement system with the sample heated by acetylene flame, and used alumina ceramic materials of 90% purity as the support plate after sintered at high temperature. In this study, the temperature upper limit can be adjusted by the mixing ratio of oxygen and acetylene, while the highest temperature is 2700~3000 °C when the mixing ratio is less than 1.1, the highest temperature is 2800~3200 °C when the mixing ratio is 1.1~1.2 and the highest temperature is 3100~3300 °C when the mixing ratio is greater than 1.2. As the thermal conductivity of the sample to be tested was low, sample thickness was selected as 3 mm, and the Christiansen wavelength temperature measurement method was adopted for dielectric materials such as SiC and MgO in the wavelength range of 2~25  $\mu\text{m}$  and the temperature range of 800~1500 °C.

With the development of the radiation heating field, laser heating and xenon lamp heating is more and more widely used. This heating method has no upper limit of temperature, as long as the power of laser or xenon lamp increases, and the non-contact heating method will not cause pollution to the sample. However, there are some problems in radiation heating methods, for example, the diameter of laser heating source is small and the

energy distribution satisfies Gaussian distribution, which needs to be expanded and energy homogenized in the application, and this problem also exists in xenon lamp heating, which needs to make a defocus adjustment on the xenon lamp to achieve uniform distribution of focal plane energy. In addition, the data of heating laser wavelength and heating band of the xenon lamp should be removed from the measurement results when the emission spectrum measurement is carried out for semitransparent materials, so as to remove the radiation interference from the radiation heating source. In 1999 [77], the High Temperature Materials Research Center of the National Research Center of France carried out experimental research on the high-temperature radiation characteristics of semitransparent materials, with the experimental systems shown in Figure 19, which took the CO<sub>2</sub> laser as the heating device and the Bruker IFS 113V FTIR spectrometer as the light source and detection device in the wavelength range of 0.83~1000 μm and the temperature range of 600~3000 K. The samples in this study included SiO<sub>2</sub>, MgO, Al<sub>2</sub>O<sub>3</sub> and Al<sub>2</sub>O<sub>3</sub> ceramics. In order to eliminate the axial temperature gradient of the sample, a beam splitter was used to divide the laser beam into two equal beams, and the surface on both sides of the sample was heated at the same time, while the thickness of the sample was less than 2 mm. In addition, in order to eliminate the radial temperature gradient of the sample, the sample was placed in the isothermal region of the beam. In 2007 [78], this system was used to measure the directional emissivity of SiO<sub>2</sub> glass containing bubbles in the wavelength range of 2~25 μm at 1300 K. In 2011 [79], the system was improved to simultaneously measure the emission spectra of blackbody furnace and high-temperature samples by using two spectrometers, as shown in Figure 20. Based on this system, the directional emissivity of YSH ceramics with a thickness of 3 mm was measured in the wavelength range of 0.57~167 μm and the temperature range of 580~2350 K. In 2015 [80], Meneses et al. built an apparatus for measuring the emittance of materials based on a CO<sub>2</sub> laser heating system and two spectrometers, and this measuring system was used to obtain the emittance of low-porosity ceramics up to 1573 K in 2021 [81].

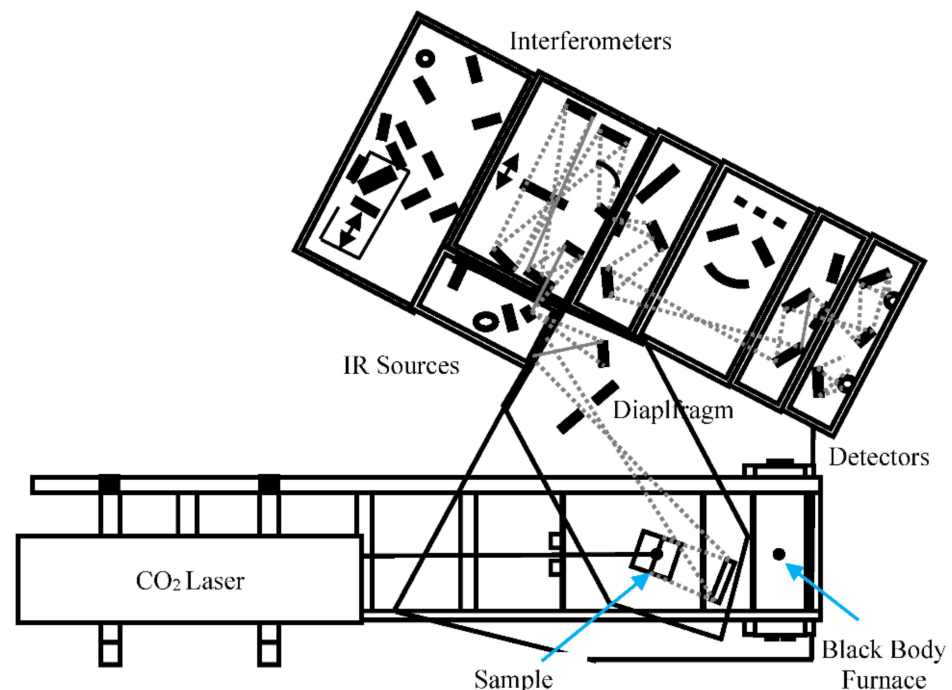


**Figure 19.** Measuring system for high-temperature emissivity [77].

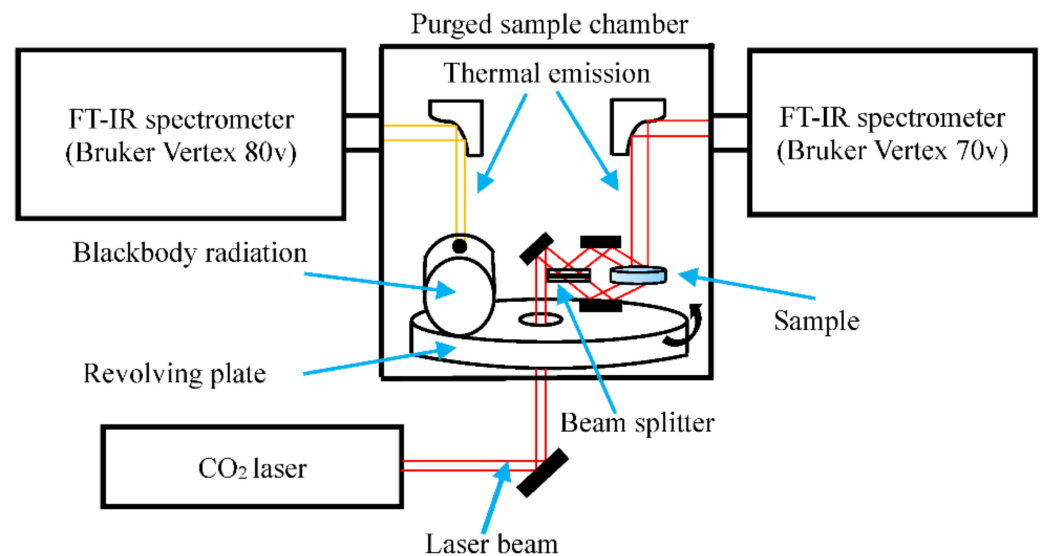
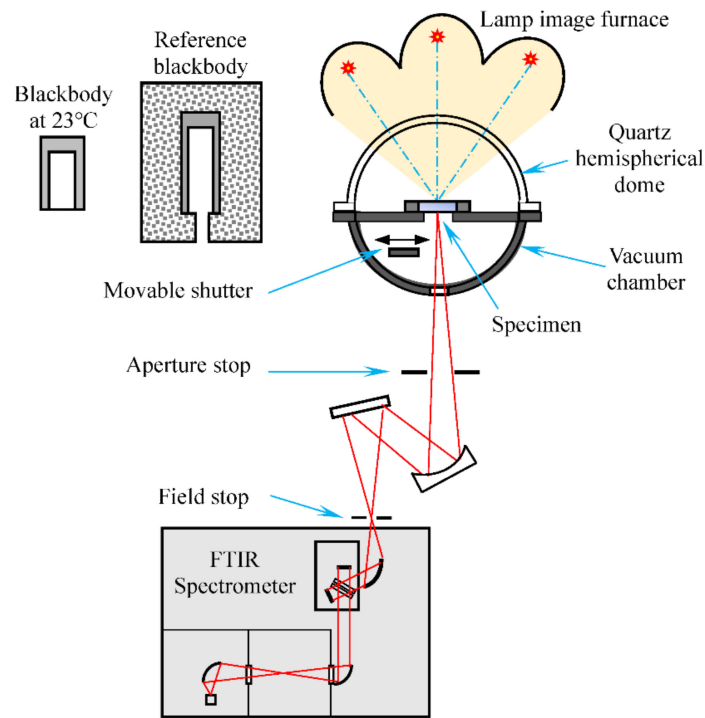


Figure 20. Improved measuring system for high-temperature emissivity [79].

The spectral energy distribution of a filtered xenon lamp is close to the solar radiation, which can be used to build a solar simulator, and the radiation intensity can be adjusted by changing the number and power of xenon lamps. The solar simulator is usually used for photothermal performance conversion and photocatalytic performance research, until some researchers introduce it into the experimental research of high-temperature emission characteristics as a radiation heating source. L. Robin [82,83] et al. set up the experimental system for high-temperature emission characteristic measurements, which included three parts: the heating device of four-xenon lamp furnace, the optical transmission system and the FTIR spectrometer detection device used to measure the emission factors of semitransparent materials. In the experiment, the Pyrex filter was used to prevent the xenon lamp spectrum within the wavelength of  $2.7\ \mu\text{m}$  from interfering with measurement results, and the emission spectrum of samples was only measured in the wavelength range of  $2.7\sim 15\ \mu\text{m}$ . Considering that the xenon lamp radiation intensity met Gaussian distribution, which would cause a radial temperature gradient on the sample, the defocus adjustment was adopted to obtain the uniform temperature zone with a certain area, but the axial temperature gradient could not be removed due to the heat transfer characteristics of the sample itself, so this study performed emission spectrum measurements on both sides of the sample in the wavelength range of  $2.5\sim 15\ \mu\text{m}$ . Bruno [84] et al. from the French National Laboratory of Measurement and Measurement (LNE-LCM) built a high-temperature emission measurement system based on the seven-halogen-lamp array furnace (single lamp 400 W), as shown in Figure 21, which concentrated the radiation energy of the lamp array furnace on the sample (diameter 25 mm, thickness 10 mm) by an elliptical mirror and detected the emission signal on the unheated side of sample under inert atmosphere in the wavelength range of  $0.8\sim 10\ \mu\text{m}$  up to  $1500\ ^\circ\text{C}$ . Fu [85] et al. from Tsinghua University used a six-quartz-lamp array as the radiation heating source, and measured the emissivity curve of a 99.9% pure non-graphite oxide sample at  $878.5\ \text{K}$  in the wavelength range of  $1.15\sim 1.60\ \mu\text{m}$  based on the verification of this experimental system by diffuse Teflon material with known direction-hemispherical reflectance.



**Figure 21.** The seven-halogen-lamp array furnace [84].

In addition to above heating methods, in 2011 [86], the Bavarian Applied Energy Research Center in Germany proposed to use the blackbody boundary method (BBC) to measure the emissivity of samples, whose principle was measuring and calculating the temperature and emissivity of a sample by changing the boundary conditions between the front and back hemispheres of the sample as shown in Figure 22. In this study, the samples were measured by an FTIR spectrometer in the wavelength range of 4–18  $\mu\text{m}$  and the temperature range of 300–1100 K, including three kinds of oxidized ceramics ( $\text{MgO}$ ,  $\text{Al}_2\text{O}_3/\text{ZrO}_2$ ,  $\text{TiO}_2/\text{Y}_2\text{O}_3$ ) and SiC ceramics. However, the temperature homogenization of the sample was not explained. In 2013 [87], Wang from North China Electric Power University used a heat gun to heat materials with low thermal conductivity and carried out emissivity measurement research in the wavelength range of 2–14  $\mu\text{m}$  and the temperature range of 150–750  $^\circ\text{C}$ .

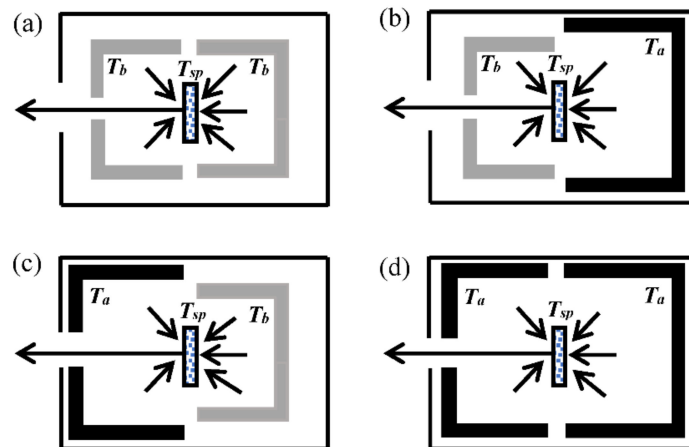


**Figure 22.** Schematic of temperature and emissivity measurements by the blackbody boundary condition (BBC) method, which (a–d) exhibits the different directional-hemispherical transmittance and reflectance) [86].

Except for studies only related to the radiation process, some researchers [88–91] choose to couple conductive and radiative heat transfer and the radiative conductivity is used based on the Rosseland approximation. The transient plane source technique is often used in this kind of study, which is a choice to characterize the thermal properties of materials.

#### 4. Identification Model of Spectral Radiation Characteristic Parameters

The physical quantities obtained by experimental measurements are apparent radiation characteristics of materials, but the foundation radiation characteristics need to be known in practical applications to facilitate the calculation of radiation characteristics for materials with various specifications and under all kinds of conditions, therefore, the research on spectral radiation characteristics of materials based on experimental methods includes not only the stage of experiments, but also the stage of parameter identification. For absorbing and scattering semitransparent materials, the absorption coefficient, scattering coefficient and scattering phase function (or attenuation coefficient and scattering albedo and scattering phase function) are needed to completely describe the radiation characteristics, and then different identification models for the spectral radiation characteristics parameters based on different apparent radiation characteristics are classified and summarized in the following.

##### 4.1. Identification of Radiation Characteristic Parameters Based on Transmission/Reflection Spectra

Due to the strong scattering characteristics of absorbing and scattering semitransparent materials, it is difficult to obtain all the parameters describing their complete radiation characteristics only by normal transmission spectrum data. Therefore, researchers obtain as much information as possible by measuring transmission and reflection spectra in multiple directions in practical studies. Among the currently developed identification models, some are only based on the direction-hemispherical transmission/reflection spectra, some are only based on the bi-directional transmission/reflection spectra, while some combine these two. Among them, although the identification model only based on direction-hemispherical transmission/reflection spectra is simple and rapid, the information is less, so it usually combines the signals of samples with different thicknesses or different incident angles to increase the information amount, and it can only identify the attenuation coefficient and albedo under the condition of given sample thickness and known phase function. For bi-directional spectral radiation characteristic measurement, more information is contained, and this information is more suitable to identify the radiation characteristics parameters of this kind of medium than the direction-hemispherical transmission/reflection spectra under different incident angles [25]. Theoretically, the phase function of the material can be identified according to the measurement results of the bi-directional spectral radiation characteristics, but the measurement signal is weak and noisy, except for the normal incident direction in the actual measurement, so the phase function is still difficult to identify. Based on the above analysis, the functional form of the scattering phase, the relationship between parameters to be identified and measured physical quantities and the amount of experimental measurement data required for identification are mainly analyzed and demonstrated for the actual research on radiation characteristic parameter identification of absorbing and scattering semitransparent materials.

In 1994 [92], Nicolau et al. measured the normal-directional transmission/reflection spectra of fiber insulation materials at several angles, and the sample's own emission was not considered in the radiation transmission process as the incident radiation was modulated. The phase function in the form of Legendre polynomials is mostly used in the traditional methods, but there may be a large number of unknown parameters to be determined for participating media such as fiber and foam. Therefore, the combination of two H-G phase functions and the isotropic phase function was used in this study, involving four unknown parameters, while expressions of objective function and phase function are shown in Equations (1) and (2), respectively. The optical thickness (i.e., the

attenuation coefficient) was directly identified by Beer's law only through the collimated transmission part of the normal transmittance, while the scattering transmission part of the measurement results needed to be extrapolated by second-order polynomial according to the scattering transmittances in the two directions closest to the incident direction, as shown in Equation (3). Then, according to the results of sensitivity analysis, parameter value  $g_2$  could be given in advance as it had less impact on other parameters, while other parameters were determined by minimizing the deviation between measured and theoretical values. In this study, transmission spectra in 11 directions and reflection spectra in 6 directions were adopted in the wavelength range of 0.5~5.5  $\mu\text{m}$ , and it was indicated that this identification method was suitable for materials with optical thickness less than 13 or 14. In 2002 [25], Sacadura and Baillis et al. adopted the same phase function form as Nicolau, while the objective function is shown in Equation (4). Sensitivity analysis of this study showed that scattering albedo is sensitive to hemispherical transmittance and hemispherical reflectance, but it is insufficient to conduct spectral radiation characteristic identification only on the basis of hemispherical transmittance and hemispherical reflectance, especially the identification of phase function, therefore, Baillis et al. combined the direction-hemispherical and bi-directional signals to identify the spectral radiant characteristics of polyurethane foam in 2002 [24], while only six transmission spectra in the directions close to incident direction and hemispherical transmittance/reflectance were chosen for identification due to the weak energy and strong noise in other directions in the wavelength range of 2.2~15.3  $\mu\text{m}$ . The scattering phase function adopted the form of an H-G phase function, as shown in Equation (5), where only one unknown parameter was involved, and the objective function is shown in Equation (6). In this study, the influence of the number of transmission spectra and measurement errors on the identification results was also analyzed, which indicated that the influence of experimental errors on the identification results was very small and the higher the number of transmission spectra used, the better the convergence of identification results. In 2002 [24], Baillis et al. compared the differences in identification using different measurement data, and this research indicated that the form of scattering phase function chosen for identification almost had no effect on the calculation results of the weighted attenuation coefficient, while the weighted scattering albedo was quite different, therefore, the method combining the directional and hemispherical transmittance/reflection spectra was more reliable in practical applications. The same year [29], Milandri et al. found there was certain deviation between the calculation results of scattering phase function by Equation (2) and Mie theory, and proposed a new expression for the scattering phase function as shown in Equations (7) and (8), which contains six parameters to be identified, except the optical thickness. Then, by sensitivity coefficient analysis,  $g_{\text{Lorentz},\lambda}$  and  $f_{3,\lambda}$  were set as constants and only four parameters needed to be identified. In addition, Marti [31] et al. adopted a double Henyey-Greenstein (DHG) phase function with both a back-scattering peak and forward-scattering peak for SiC particle suspensions as shown in Equation (9), while Germilly [93] et al. estimated the asymmetry factor of the H-G scattering phase function for porous volumetric receivers made of open-cell SiC ceramic foam through experiments and simulations of hemispherical diffuse reflectance.

$$F(\tau_0, \omega, g_1, g_2, f_1, f_2) = \sum_{i=1}^N [T_{ti}(\tau_0, \omega, g_1, g_2, f_1, f_2) - T_{ei}] \quad (1)$$

$$p_v(\mu', \mu) = f_1 f_2 p_{HG, g_1}(\mu', \mu) + (1 - f_1) f_2 p_{HG, g_2}(\mu', \mu) + (1 - f_2) \quad (2)$$

$$\left(T_{\lambda, \text{exp}}^d\right)_1 = \left(\left(T_{\lambda, \text{exp}}^d\right)_2 - \left(T_{\lambda, \text{exp}}^d\right)_3\right) \left\{ \frac{(\mu_1^2 - \mu_2^2) - 2\mu_1(\mu_1 - \mu_2)}{(\mu_2^2 - \mu_3^2) - 2\mu_1(\mu_2 - \mu_3)} \right\} + \left(T_{\lambda, \text{exp}}^d\right)_2 \quad (3)$$

$$F(p_1, \dots, p_n) = \sum_{i=1}^N [T_{ti}(p_1, \dots, p_n) - T_{ei}]^2 \quad (4)$$

$$\Phi_{\lambda}(\theta) = \frac{1 - g_{\lambda}^2}{(1 + g_{\lambda}^2 + 2g_{\lambda} \cos \theta)^{1.5}} \quad (5)$$

$$F(\omega, \beta, g) = \sum_{i=1}^N \left[ \frac{T_{ti}(\omega, \beta, g) - T_{ei}}{T_{ei}} \right]^2 \quad (6)$$

$$p_{\lambda}(\xi_i, \xi_j) = (1 - f_{3,\lambda})P_{Nicolau,\lambda}(\mu_i, \mu_j) + f_{3,\lambda}P_{Lorentz,\lambda}(\xi_i, \xi_j) \quad (7)$$

$$P_{Lorentz,\lambda}(\xi_i, \xi_j) = \frac{1}{\pi} \frac{g_{Lorentz,\lambda}}{g_{Lorentz,\lambda}^2 - (\xi_j - \xi_i)^2} \quad (8)$$

$$\Phi_{DHG}(\theta_s, g_1, g_2, \alpha) = \alpha \Phi_{HG}(g_1, \theta_s) + (1 - \alpha) \Phi_{HG}(-g_2, \theta_s) \quad (9)$$

where  $\xi_i$  and  $\xi_j$  stand for polar angle of incident and scattering direction, respectively.

In 2004 [26], Baillis et al. studied the radiation characteristics of SiO<sub>2</sub> glass containing bubbles, and measured the transmission spectra in eight directions and reflection spectra in three directions in the wavelength range of 1.67~3.5  $\mu\text{m}$ . The scattering phase function was in the form of an H-G phase function, and the RTE in identification was discrete in 24 directions. According to the identification results, the attenuation coefficient identified from the sample with 3 mm thickness deviated from other cases, which may be because the sample was too thin to be regarded as homogeneous medium because of internal bubbles, which had been reported by Hale and Bohn based on open-cell alumina foams. In 2006 [94], Randrianalisoa and Baillis et al. pointed out that the scattering phase function in the form of Legendre polynomials is not suitable for strongly anisotropic materials as it involves a large number of unknown parameters, and therefore, they proposed the TPF polynomials as shown in Equation (10), which contain three unknown parameters. For the identification of the attenuation coefficient, Equation (11) was used to characterize the collimation transmission ratio, and the scattering transmission part was estimated by third-order polynomial, as shown in Equation (12).

$$\begin{cases} \Phi_{\lambda}(\Theta, f_1, g_1, g_2) = \Phi_{1\lambda}(\Theta, f_1, g_1, g_2) = f_1 \Phi_{HG\lambda}(\Theta, g_1) + (1 - f_1) \Phi_{HG\lambda}(\Theta, g_2) & \text{for } 0 \leq \Theta \leq \pi/2 \\ \Phi_{\lambda}(\Theta, f_1, g_1, g_2) = 0.03 \Phi_{1\lambda}(\Theta, f_1, g_1, g_2) & \text{elsewhere} \end{cases} \quad (10)$$

$$T_{coll} = T_{e1} - T_{sca1} = \frac{(1 - r_{12})^2 \exp(-\beta e)}{1 - r_{12}^2 \exp(-2\beta e)} \quad (11)$$

$$T_{scai} = \varepsilon_3 \eta_i^3 + \varepsilon_2 \eta_i^2 + \varepsilon_1 \eta_i + \varepsilon_0 \quad (12)$$

In 2008 [95], Loretz et al. further pointed out in radiation property research for aluminum foam that the normal-normal transmittance was strongly correlated with the attenuation coefficient, but weakly varied with the scattering albedo and the mirror-diffuse reflection ratio in the phase function, and the sum of hemispheric transmission spectrum and hemispheric reflection spectra represents the fraction of incident energy leaving the sample, so it mainly depends on the scattering albedo. In addition, the ratio of hemispherical reflectance spectrum to hemispherical transmission spectrum varies with the diffuse reflectance ratio. The aluminum foam sample was regarded as semitransparent medium with absorbing and scattering properties, and the scattering phase function adopted the combination form between the scattering phase function of a diffuse sphere, based on Mie theory, and the isotropic phase function, as the ratio between these two parts were adjusted by the mirror-diffuse reflectance ratio parameter, which is shown in Equations (13)–(15). This research indicated that the attenuation coefficient is almost independent of the wavelength, which confirms that the law of geometric optics can be used to determine the radiation characteristics of the foam. In addition, the mirror-diffuse reflectance ratio parameter was approximately zero for most wavelengths, indicating that the scattering characteristics of aluminum foam was close to the scattering behavior of diffuse opaque spheres.

$$\Phi_{\lambda}(\theta) = ps_{\lambda} \times \Phi_{spec,\lambda}(\theta) + (1 - ps_{\lambda}) \times \Phi_{dif,\lambda}(\theta) \quad (13)$$

$$\Phi_{dif,\lambda}(\theta) = \frac{8}{3\pi} \times (\sin \theta - \theta \times \cos \theta) \quad (14)$$

$$\Phi_{spec,\lambda}(\theta) = 1 \quad (15)$$

For the identification of the extinction coefficient, one method is based on the normal transmittance, as there exists a strong correlation between these two physical quantities. Loretz [14] et al. proposed a more convenient method, which determined the directional transmittance by the ratio of remaining white pixels to the total surface of the plane obtained from X-ray tomography, and calculated the extinction coefficient in different directions based on Beer's Law simply by rotating the sample before using this method. Also based on Beer's Law, Liu [96] et al. proposed the three-layer structure model to describe the radiation transfer process in open-cell metallic foams, which took the broken frame mechanism on cut surfaces into account, and determined the real extinction coefficient by the double-thickness normal transmission method based on this model. Except determining the extinction coefficient by Beer's Law, Amine [97] et al. calculated the spectral absorptivity from the hemispherical transmittance and hemispherical reflectance. The other method is based on geometrical parameters of microstructures. Lisa [98] et al. compared several prediction models for the extinction coefficient of ceramic open-cell foams used for metal melt filtration.

In 2012 [38], Coquard et al. used tomographic images and SEM scanning images to study the radiation characteristics of Al-NiP foam materials, and pointed out that the superiority of using tomographic scanning technology compared to analytical models was not evaluated in previous studies. For the open-cell foams with opaque skeletons, the lights that reached the solid phase were truncated, absorbed or reflected, therefore, the attenuation coefficient only depended on the structure characteristics of the foam, and was irrelevant with the wavelength, optical property of the solid phase and surface roughness. In this paper, the numerical calculation results and the predicted results based on the analytical model were compared and indicated that the analytical model could obtain accurate results when choosing the appropriated parameters, but this adjustment parameter was difficult to obtain accurately.

In addition to the above-mentioned studies that take the absorption coefficient, scattering coefficient and scattering phase function parameters of absorbing and scattering semitransparent materials as the identification objects, some researchers also carry out the identification of corresponding parameters based on self-constructed prediction models. For example, Baillis used the data of bi-directional transmission spectra and reflection spectra at several directions and wavelengths measured experimentally in 1999 [23] to identify the radiation characteristic parameters of carbon foam based on the D-S prediction model proposed by Doermann et al. in 1996 [99]. This prediction model first combined geometrical optics and diffraction theory, and described the particle radiative interaction in foams, which was the function of the shape parameters, the porosity, thermal characteristics of solid phase and gas phase and the optical properties of solid phase, and could be used to predict the spectral absorption coefficient, scattering coefficient and volume scattering phase function.

#### 4.2. Identification of Radiation Characteristic Parameters Based on Emission Spectrum

As the measurement systems of directional radiation characteristics mostly work at room temperature, the measurement of radiation characteristics at high temperature is mainly emission measurement. But research devoted to emission measurements usually focuses on accurately obtaining the emissivity of a sample as the stray radiation cannot be eliminated at the source, thus the research on identification of radiation characteristic parameters based on emission spectra are less.

In 2011 [100], Domebrovsky et al. used CO<sub>2</sub> laser heating to measure the normal emissivity of 8YSZ samples at the temperature of 1700 K, and assumed that the porosity, refractive index and transmission scattering coefficient of samples were weakly correlated with temperature. On this basis, the variation of normal emissivity with temperature

was attributed to the variation of the absorption coefficient with temperature, and the absorption coefficient was obtained by the analytical expression of emissivity.

In 2013 [71], the normal emissivity of porous alumina ceramics was measured based on the double substrate method in South Korea, and the transmission and reflection spectra of porous alumina ceramics were obtained according to the characteristics of the substrate material, and then the attenuation coefficient spectra were calculated based on the Lambert-Beer law.

In 2016 [101], Simon et al. studied the representative volume (REV) of normal spectral emissivity for SiC foam and pointed out that it could not be used as REV if the volume was too small. Considering it is difficult to determine the link between the absorption characteristics and REV for real open-cell foams with a large number of morphological characteristics by experimental means, 3D virtual samples were selected to analyze the influence of morphological characteristics on the porosity REV and emissivity REV, and eventually the correlation between the emissivity, the porosity and the optical constants of base material were fitted.

## 5. Conclusions and Prospect

The research on spectral radiation characteristics of materials usually includes experimental measurement and parameter identification. Due to the structure complexity of absorbing and scattering semitransparent materials, the traditional methods for radiation characteristic measurement can no longer meet the research needs. Therefore, researchers have built and improved the radiation characteristic measurement systems for this kind of material. Due to the limitations of the performance of experimental components, bi-directional transmission/reflection and direction-hemispherical transmission/reflection measurements are mostly carried out at room temperature, while the measurement at high temperature mainly adopts the emission method.

Although bi-directional transmission/reflection spectrum measurement can supply more information for the identification of radiation characteristics of this kind of material, the directional signals are weak in directions deviated from the incident direction and are difficult to distinguish. At the same time, it is insufficient to identify only based on the direction-hemispherical transmission/reflection spectra, therefore, researchers select to combine these two signals and obtain a satisfactory result. The radiation characteristic parameters to be identified for absorbing and scattering semitransparent materials mainly include the absorption coefficient, scattering coefficient and scattering phase function, among which the accurate expression of scattering phase function is of great importance. Considering that the traditional scattering phase function expressed by Legendre polynomial is relatively cumbersome, and more unknown parameters are introduced into the identification process, researchers put forward some simplified expressions of scattering phase function for some kinds of absorbing and scattering semitransparent materials, which are verified by experiments or numerical methods. Based on this, other researchers can select the simplified scattering phase function expression in future studies when the sample to be tested has a similar structure to previous research. However, if no similar reports have been found for the studied materials, the combination of multiple simplified scattering phase function expressions can be used to obtain the scattering distribution as accurately as possible by setting several unknown parameters. Under the condition that the expression of the scattering phase function is determined, a numerical simulation program according to the measurement process is established based on the radiative transfer equation (RTE), and then the difference between the measured and calculated physical quantities is minimized through the optimization algorithm, so as to obtain the spectral radiation characteristic parameters of materials.

In contrast, there are few studies on the measurement of the spectral radiation characteristics of absorbing and scattering semitransparent materials at high temperatures. Except for the high temperature measurement of the direction-hemispherical reflection spectra carried out in Russia, the other studies are mainly based on emission measurements.

Considering the light source in emission measurement is the sample itself, which cannot be modulated, and high-temperature heating exhibits many problems such as the pollution problem of flame heating, the temperature homogeneity problem of radiation heating and so on, the main focus of this research is on analysis of the physical meaning of measuring signal, the accuracy of temperature measurement and the extraction of real emissivity of a sample, then there are few studies on the identification of radiation characteristics of absorbing and scattering semitransparent materials based on emission spectra.

Based on the above analysis, although some progress has been made in the measurements of absorbing and scattering semitransparent materials, the accurate description of scattering phase function, the accurate measurement of high-temperature radiation characteristics and the identification of radiation characteristic parameters still need researchers to make efforts.

**Author Contributions:** Conceptualization, Q.A., J.G. and Y.S.; methodology, M.L., Q.A. and Y.S.; formal analysis, S.D. and J.G.; investigation, M.L. and S.D.; resources, Q.A. and J.G.; writing—original draft preparation, M.L., S.D. and Q.A.; writing—review and editing, M.L., Q.A. and J.G.; visualization, M.L. and S.D.; supervision, Q.A., J.G. and Y.S.; project administration, Q.A. and Y.S.; funding acquisition, Q.A. and Y.S. All authors have read and agreed to the published version of the manuscript.

**Funding:** This work was supported by the National Major Scientific Instruments and Equipments Development Project of National Natural Science Foundation of China (NSFC) [No. 52227813] and the National Key R&D Program of China [No. 2022YFC2204300].

**Data Availability Statement:** Public databases.

**Conflicts of Interest:** The authors declare no conflict of interest.

## References

1. Rashidi, S.; Esfahani, J.A.; Rashidi, A. A review on the applications of porous materials in solar energy systems. *Renew. Sustain. Energy Rev.* **2017**, *73*, 1198–1210. [[CrossRef](#)]
2. Anirudh, K.; Dhinakaran, S. Performance improvement of a flat-plate solar collector by inserting intermittent porous blocks. *Renew. Energy* **2020**, *145*, 428–441. [[CrossRef](#)]
3. Liu, D.; Li, Q.; Xuan, Y. Reticulated porous volumetric solar receiver designs guided by normal absorptance and hemispherical volumetric emittance investigations. *Int. J. Heat Mass Transf.* **2017**, *114*, 1067–1071. [[CrossRef](#)]
4. Teng, L.; Xuan, Y. Thermal and hydrodynamic performance of a novel volumetric solar receiver. *Sol. Energy* **2018**, *163*, 177–188. [[CrossRef](#)]
5. Xie, T.; Xu, K.; Yang, B.; He, Y. Effect of pore size and porosity distribution on radiation absorption and thermal performance of porous solar energy absorber. *Sci. China Technol. Sci.* **2019**, *62*, 2213–2225. [[CrossRef](#)]
6. Alifanov, O.M.; Budnik, S.A.; Nenarokomov, A.V.; Salosina, M.O. Design of thermal protection based on open cell carbon foam structure optimization. *Appl. Therm. Eng.* **2020**, *173*, 115252. [[CrossRef](#)]
7. Alami, A.H.; Aokal, K.; Faraj, M. Investigating nickel foam as photoanode substrate for potential dye-sensitized solar cells applications. *Energy* **2020**, *211*, 118689. [[CrossRef](#)]
8. Patel, V.M.; Talukdar, P. Determination of radiative properties of representative and real open cell foam structures using the finite volume method. *Int. J. Therm. Sci.* **2018**, *132*, 117–128. [[CrossRef](#)]
9. Cunsolo, S.; Baillis, D.; Bianco, N. Improved Monte Carlo methods for computational modelling of thermal radiation applied to porous cellular materials. *Int. J. Therm. Sci.* **2019**, *137*, 161–179. [[CrossRef](#)]
10. Li, Y.; Xia, X.-L.; Ai, Q.; Sun, C.; Tan, H.-P. Pore-level determination of spectral reflection behaviors of high-porosity metal foam sheets. *Infrared Phys. Technol.* **2018**, *89*, 77–87. [[CrossRef](#)]
11. Li, Y.; Chen, H.-W.; Xia, X.-L.; Ma, G.-Y.; Tan, H.-P. Prediction of high-temperature radiative properties of copper, nickel, zirconia, and alumina foams. *Int. J. Heat Mass Transf.* **2020**, *148*, 119154. [[CrossRef](#)]
12. Bargmann, S.; Klusemann, B.; Markmann, J.; Schnabel, J.E.; Schneider, K.; Soyarslan, C.; Wilmers, J. Generation of 3D representative volume elements for heterogeneous materials: A review. *Prog. Mater. Sci.* **2018**, *96*, 322–384. [[CrossRef](#)]
13. Liu, Y.B.; Jin, R.; Qiu, J.; Liu, L.H. Spectral radiative properties of a nickel porous microstructure and magnetic polariton resonance for light trapping. *Int. J. Heat Mass Transf.* **2016**, *98*, 833–844. [[CrossRef](#)]
14. Loretz, M.; Maire, E.; Baillis, D. Analytical Modelling of the Radiative Properties of Metallic Foams: Contribution of X-ray Tomography. *Adv. Eng. Mater.* **2008**, *10*, 352–360. [[CrossRef](#)]
15. Petrasch, J.; Wyss, P.; Stämpfli, R.; Steinfeld, A. Tomography-Based Multiscale Analyses of the 3D Geometrical Morphology of Reticulated Porous Ceramics. *J. Am. Ceram. Soc.* **2008**, *91*, 2659–2665. [[CrossRef](#)]

16. Zeng, J.S.Q.; Greif, R.; Stevens, P.; Ayers, M.; Hunt, A. Effective optical constants  $n$  and  $\kappa$  and extinction coefficient of silica aerogel. *J. Mater. Res.* **1996**, *11*, 687–693. [[CrossRef](#)]
17. Cheng, Q.; Yang, P.; Zhang, Z. Radiative Properties of Ceramic Al<sub>2</sub>O<sub>3</sub>, AlN, and Si<sub>3</sub>N<sub>4</sub>: I. Experiments. *Int. J. Thermophys.* **2016**, *37*, 62. [[CrossRef](#)]
18. Wei, G.; Liu, Y.; Zhang, X.; Yu, F.; Du, X. Thermal conductivities study on silica aerogel and its composite insulation materials. *Int. J. Heat Mass Transf.* **2011**, *54*, 2355–2366. [[CrossRef](#)]
19. Wei, G.; Liu, Y.; Zhang, X.; Du, X. Radiative heat transfer study on silica aerogel and its composite insulation materials. *J. Non-Cryst. Solids* **2013**, *362*, 231–236. [[CrossRef](#)]
20. Wei, G.; Huang, P.; Xu, C.; Chen, L.; Ju, X.; Du, X. Experimental study on the radiative properties of open-cell porous ceramics. *Sol. Energy* **2017**, *149*, 13–19. [[CrossRef](#)]
21. Dietrich, B.; Fishedick, T.; Heissler, S.; Weidler, P.G.; Wöll, C.; Kind, M. Optical parameters for characterization of thermal radiation in ceramic sponges—Experimental results and correlation. *Int. J. Heat Mass Transf.* **2014**, *79*, 655–665. [[CrossRef](#)]
22. Liu, M.; Ai, Q.; Wang, S.; Shuai, Y. Analysis on influence factors for transmission measurements of absorbing and scattering media based on the internal optical-path of FTIR spectrometer. *Measurement* **2022**, *203*, 111963. [[CrossRef](#)]
23. Baillis, D.; Raynaud, M.; Sacadura, J.F. Spectral Radiative Properties of Open-Cell Foam Insulation. *J. Thermophys. Heat Transf.* **1999**, *13*, 292–298. [[CrossRef](#)]
24. Baillis, D.; Arduini-Schuster, M.; Sacadura, J.F. Identification of spectral radiative properties of polyurethane foam from hemispherical and bi-directional transmittance and reflectance measurements. *J. Quant. Spectrosc. Radiat. Transf.* **2002**, *73*, 297–306. [[CrossRef](#)]
25. Sacadura, J.F.; Baillis, D. Experimental characterization of thermal radiation properties of dispersed media. *Int. J. Therm. Sci.* **2002**, *41*, 699–707. [[CrossRef](#)]
26. Baillis, D.; Pilon, L.; Randrianalisoa, J.; Gomez, R.; Viskanta, R. Measurements of radiation characteristics of fused quartz containing bubbles. *J. Opt. Soc. Am. A* **2004**, *21*, 149–159. [[CrossRef](#)]
27. Zeghondy, B.; Iacona, E.; Taine, J. Experimental and RDFI calculated radiative properties of a mullite foam. *Int. J. Heat Mass Transf.* **2006**, *49*, 3702–3707. [[CrossRef](#)]
28. Zhang, W.J.; Zhao, J.; Liu, L.H. Experimental Study of the Effective BRDF of a Copper Foam Sheet. In Proceedings of the 7th International Symposium on Radiative Transfer, Kusadasi, Turkey, 2–8 June 2013. Volume RAD-13-SH4.
29. Milandri, A.; Asllanaj, F.; Jeandel, G. Determination of radiative properties of fibrous media by an inverse method—Comparison with the Mie theory. *J. Quant. Spectrosc. Radiat. Transf.* **2002**, *74*, 637–653. [[CrossRef](#)]
30. Coray, P.S.; Lipiński, W.; Steinfeld, A. Spectroscopic Goniometry System for Determining Thermal Radiative Properties of Participating Media. *Exp. Heat Transf.* **2011**, *24*, 300–312. [[CrossRef](#)]
31. Marti, J.; Roesle, M.; Steinfeld, A. Experimental Determination of the Radiative Properties of Particle Suspensions for High-Temperature Solar Receiver Applications. *Heat Transf. Eng.* **2014**, *35*, 272–280. [[CrossRef](#)]
32. Good, P.; Cooper, T.; Querci, M.; Wiik, N.; Ambrosetti, G.; Steinfeld, A. Spectral reflectance, transmittance, and angular scattering of materials for solar concentrators. *Sol. Energy Mater. Sol. Cells* **2016**, *144*, 509–522. [[CrossRef](#)]
33. Ganesan, K.; Dombrovsky, L.A.; Lipiński, W. Visible and near-infrared optical properties of ceria ceramics. *Infrared Phys. Technol.* **2013**, *57*, 101–109. [[CrossRef](#)]
34. Ganesan, K.; Lipiński, W. Experimental Determination of Spectral Transmittance of Porous Cerium Dioxide in the Range 900–1700 nm. *J. Heat Transf.* **2011**, *133*, 104501. [[CrossRef](#)]
35. Zhao, C.Y.; Lu, T.J.; Hodson, H.P. Thermal radiation in ultralight metal foams with open cells. *Int. J. Heat Mass Transf.* **2004**, *47*, 2927–2939. [[CrossRef](#)]
36. Yang, G.; Zhao, C.Y.; Wang, B.X. Experimental study on radiative properties of air plasma sprayed thermal barrier coatings. *Int. J. Heat Mass Transf.* **2013**, *66*, 695–698. [[CrossRef](#)]
37. Eldridge, J.I.; Spuckler, C.M. Determination of Scattering and Absorption Coefficients for Plasma-Sprayed Ytria-Stabilized Zirconia Thermal Barrier Coatings. *J. Am. Ceram. Soc.* **2008**, *91*, 1603–1611. [[CrossRef](#)]
38. Coquard, R.; Rousseau, B.; Echegut, P.; Baillis, D.; Gomart, H.; Iacona, E. Investigations of the radiative properties of Al–NiP foams using tomographic images and stereoscopic micrographs. *Int. J. Heat Mass Transf.* **2012**, *55*, 1606–1619. [[CrossRef](#)]
39. Wang, L.; Eldridge, J.; Guo, S.M. Comparison of different models for the determination of the absorption and scattering coefficients of thermal barrier coatings. *Acta Mater.* **2014**, *64*, 402. [[CrossRef](#)]
40. Wang, L.; Habibi, M.H.; Eldridge, J.I.; Guo, S.M. Infrared radiative properties of plasma-sprayed BaZrO<sub>3</sub> coatings. *J. Eur. Ceram. Soc.* **2014**, *34*, 3941–3949. [[CrossRef](#)]
41. Burger, T.; Kuhn, J.; Caps, R.; Fricke, J. Quantitative Determination of the Scattering and Absorption Coefficients from Diffuse Reflectance and Transmittance Measurements: Application to Pharmaceutical Powders. *Appl. Spectrosc.* **1997**, *51*, 309–317. [[CrossRef](#)]
42. Burger, T.; Fricke, J.; Kuhn, J. NIR radiative transfer investigations to characterise pharmaceutical powders and their mixtures. *J. Near Infrared Spectrosc.* **1998**, *6*, 33. [[CrossRef](#)]
43. Manara, J.; Caps, R.; Raether, F.; Fricke, J. Characterization of the pore structure of alumina ceramics by diffuse radiation propagation in the near infrared. *Opt. Commun.* **1999**, *168*, 237–250. [[CrossRef](#)]

44. Baillis, D.; Raynaud, M.; Sacadura, J.F. Determination of Spectral Radiative Properties of Open Cell Foam: Model Validation. *J. Thermophys. Heat Transf.* **2000**, *14*, 137–143. [[CrossRef](#)]
45. Baillis, D.; Sacadura, J. Identification of polyurethane foam radiative properties-influence of transmittance measurements number. *J. Thermophys. Heat Transf.* **2002**, *16*, 200–206. [[CrossRef](#)]
46. Dombrovsky, L.A.; Tagne, H.K.; Baillis, D.; Gremillard, L. Near-infrared radiative properties of porous zirconia ceramics. *Infrared Phys. Technol.* **2007**, *51*, 44–53. [[CrossRef](#)]
47. Coquard, R.; Baillis, D.; Quenard, D. Numerical and experimental study of the IR opacification of polystyrene foams for thermal insulation enhancement. *Energy Build.* **2019**, *183*, 54–63. [[CrossRef](#)]
48. Reidinger, M.; Rydzek, M.; Scherdel, C.; Arduini-Schuster, M.; Manara, J. Low-emitting transparent coatings based on tin doped indiumoxide applied via a sol-gel routine. *Thin Solid Film.* **2009**, *517*, 3096–3099. [[CrossRef](#)]
49. Rydzek, M.; Reidinger, M.; Arduini-Schuster, M.; Manara, J. Low-emitting surfaces prepared by applying transparent aluminum-doped zinc oxide coatings via a sol-gel process. *Thin Solid Film.* **2012**, *520*, 4114–4118. [[CrossRef](#)]
50. Manara, J.; Arduini-Schuster, M.; Rätzer-Scheibe, H.-J.; Schulz, U. Infrared-optical properties and heat transfer coefficients of semitransparent thermal barrier coatings. *Surf. Coat. Technol.* **2009**, *203*, 1059–1068. [[CrossRef](#)]
51. Rydzek, M.; Reidinger, M.; Arduini-Schuster, M.; Manara, J. Comparative study of sol-gel derived tin-doped indium- and aluminum-doped zinc-oxide coatings for electrical conducting and low-emitting surfaces. *Prog. Org. Coat.* **2011**, *70*, 369–375. [[CrossRef](#)]
52. Manara, J.; Reidinger, M.; Rydzek, M.; Arduini-Schuster, M. Polymer-based pigmented coatings on flexible substrates with spectrally selective characteristics to improve the thermal properties. *Prog. Org. Coat.* **2011**, *70*, 199–204. [[CrossRef](#)]
53. Arduini-Schuster, M.; Manara, J.; Vo, C. Experimental characterization and theoretical modeling of the infrared-optical properties and the thermal conductivity of foams. *Int. J. Therm. Sci.* **2015**, *98*, 156–164. [[CrossRef](#)]
54. Arduini, M.; Manara, J.; Vo, C. Modeling of Radiative Properties of Polystyrene Foams Containing IR-Opacifiers. *Cell. Polym.* **2016**, *35*, 49–66. [[CrossRef](#)]
55. Zhao, L.; Yang, S.; Bhatia, B.; Strobach, E.; Wang, E.N. Modeling silica aerogel optical performance by determining its radiative properties. *AIP Adv.* **2016**, *6*, 025123. [[CrossRef](#)]
56. Li, Q.; Fan, D.; Xuan, Y. Thermal radiative properties of plasma sprayed thermochromic coating. *J. Alloy. Compd.* **2014**, *583*, 516–522. [[CrossRef](#)]
57. Sani, E.; Landi, E.; Sciti, D.; Medri, V. Optical properties of ZrB<sub>2</sub> porous architectures. *Sol. Energy Mater. Sol. Cells* **2016**, *144*, 608–615. [[CrossRef](#)]
58. Sani, E.; Mercatelli, L.; Meucci, M.; Balbo, A.; Musa, C.; Licheri, R.; Orrù, R.; Cao, G. Optical properties of dense zirconium and tantalum diborides for solar thermal absorbers. *Renew. Energy* **2016**, *91*, 340–346. [[CrossRef](#)]
59. Sani, E.; Meucci, M.; Mercatelli, L.; Balbo, A.; Musa, C.; Licheri, R.; Orrù, R.; Cao, G. Titanium diboride ceramics for solar thermal absorbers. *Sol. Energy Mater. Sol. Cells* **2017**, *169*, 313–319. [[CrossRef](#)]
60. Soum-Glaude, A.; Le Gal, A.; Bichotte, M.; Escape, C.; Dubost, L. Optical characterization of TiAlN<sub>x</sub>/TiAlN<sub>y</sub>/Al<sub>2</sub>O<sub>3</sub> tandem solar selective absorber coatings. *Sol. Energy Mater. Sol. Cells* **2017**, *170*, 254–262. [[CrossRef](#)]
61. Jyothi, J.; Soum-Glaude, A.; Nagaraja, H.S.; Barshilia, H.C. Measurement of high temperature emissivity and photothermal conversion efficiency of TiAlC/TiAlCN/TiAlSiCN/TiAlSiCO/TiAlSiO spectrally selective coating. *Sol. Energy Mater. Sol. Cells* **2017**, *171*, 123–130. [[CrossRef](#)]
62. Akopov, F.A.; Val'vano, G.E.; Vorob'ev, A.Y.; Mineev, V.N.; Petrov, V.A.; Chernyshev, A.P.; Chernyshev, G.P. Thermal Radiative Properties of Ceramic of Cubic ZrO<sub>2</sub>Stabilized with Y<sub>2</sub>O<sub>3</sub>at High Temperatures. *High Temp.* **2001**, *39*, 244–254. [[CrossRef](#)]
63. Zhang, Y.F.; Dai, J.M.; Wang, Z.W.; Pan, W.D.; Zhang, L. A Spectral Emissivity Measurement Facility for Solar Absorbing Coatings. *Int. J. Thermophys.* **2013**, *34*, 916–925. [[CrossRef](#)]
64. White, S.M. High-Temperature Spectrometer for Thermal Protection System Radiation Measurements. *J. Spacecr. Rocket.* **2010**, *47*, 21–28. [[CrossRef](#)]
65. Eldridge, J.I.; Spuckler, C.M.; Markham, J.R. Determination of scattering and absorption coefficients for plasma-sprayed yttria-stabilized zirconia thermal barrier coatings at elevated temperatures. *J. Am. Ceram. Soc.* **2009**, *92*, 2276–2285. [[CrossRef](#)]
66. Ballico, M.J.; Jones, T.P. Novel experimental technique for measuring high-temperature spectral emissivities. *Appl. Spectrosc.* **1995**, *49*, 335–340. [[CrossRef](#)]
67. del Campo, L.; Pérez-Sáez, R.B.; Esquisabel, X.; Fernández, I.; Tello, M.J. New experimental device for infrared spectral directional emissivity measurements in a controlled environment. *Rev. Sci. Instrum.* **2006**, *77*, 113111. [[CrossRef](#)]
68. Koirala, L.R. FTIR Spectroscopic Measurement of Directional Spectral Emissivities of Microstructured Surfaces. Ph.D. Thesis, Helmut Schmidt University, Hamburg, Germany, 2004.
69. Jeon, S.; Park, S.-N.; Yoo, Y.S.; Hwang, J.; Park, C.-W.; Lee, G.W. Simultaneous measurement of emittance, transmittance, and reflectance of semitransparent materials at elevated temperature. *Opt. Lett.* **2010**, *35*, 4015–4017. [[CrossRef](#)] [[PubMed](#)]
70. Lee, G.W.; Jeon, S.; Yoo, N.J.; Park, C.W.; Park, S.-N.; Kwon, S.Y.; Lee, S.-H. Normal and Directional Spectral Emittance Measurement of Semi-Transparent Materials Using Two-Substrate Method: Alumina. *Int. J. Thermophys.* **2011**, *32*, 1234–1246. [[CrossRef](#)]
71. Jeon, S.; Kang, D.-H.; Lee, G.W. Difference of optical properties between porous alumina and sapphire using two-substrate method at elevated temperature. *Curr. Appl. Phys.* **2013**, *13*, 1594–1599. [[CrossRef](#)]

72. Li, N.; Xing, P.; Li, C.; Wang, P.; Jin, X.; Zhang, X. Influence of surface oxidation on the radiative properties of ZrB<sub>2</sub>-SiC composites. *Appl. Surf. Sci.* **2017**, *409*, 1–7. [[CrossRef](#)]
73. Lim, G.; Kar, A. Radiative properties of thermal barrier coatings at high temperatures. *J. Phys. D Appl. Phys.* **2009**, *42*, 155412. [[CrossRef](#)]
74. Rydzek, M.; Stark, T.; Arduini-Schuster, M.; Manara, J. Newly Designed Apparatus for Measuring the Angular Dependent Surface Emittance in a Wide Wavelength Range and at Elevated Temperatures up to 1400 °C. *J. Phys. Conf. Ser.* **2012**, *395*, 012152. [[CrossRef](#)]
75. Hatzl, S.; Kirschner, M.; Lippig, V.; Sander, T.; Mundt, C.; Pfitzner, M. Direct Measurements of Infrared Normal Spectral Emissivity of Solid Materials for High-Temperature Applications. *Int. J. Thermophys.* **2013**, *34*, 2089–2101. [[CrossRef](#)]
76. Wang, L. Study on the Measurement of Material Spectral Emissivity at High Temperature. Ph.D. Thesis, Nanjing University of Science & Technology, Nanjing, China, 2014.
77. Rozenbaum, O.; Meneses, D.; Auger, Y.; Chermanne, S.; Echegut, P. A Spectroscopic Method to Measure the Spectral Emissivity of Semi-Transparent Materials Up to High Temperature. *Rev. Sci. Instrum.* **1999**, *70*, 4020–4025. [[CrossRef](#)]
78. Rousseau, B.; De Sousa Meneses, D.; Echegut, P.; Di Michiel, M.; Thovert, J.-F. Prediction of the thermal radiative properties of an X-ray u-tomographed porous silica glass. *Appl. Opt.* **2007**, *46*, 4266–4276. [[CrossRef](#)] [[PubMed](#)]
79. del Campo, L.; De Sousa Meneses, D.; Blin, A.; Rousseau, B.; Véron, E.; Balat-Pichelin, M.; Echegut, P. High-Temperature Radiative Properties of an Yttria-Stabilized Hafnia Ceramic. *J. Am. Ceram. Soc.* **2011**, *94*, 1859–1864. [[CrossRef](#)]
80. Meneses, D.D.S.; Melin, P.; del Campo, L.; Cosson, L.; Echegut, P. Apparatus for measuring the emittance of materials from far infrared to visible wavelengths in extreme conditions of temperature. *Infrared Phys. Technol.* **2015**, *69*, 96–101. [[CrossRef](#)]
81. Low, Z.K.; Novikov, A.; Meneses, D.D.S.; Baillis, D. Radiative behavior of low-porosity ceramics: II—Experimental and numerical study of porous alumina up to high temperatures. *J. Quant. Spectrosc. Radiat. Transf.* **2021**, *272*, 107821. [[CrossRef](#)]
82. Delmas, A. Experimental and theoretical determination of spectral heat flux emitted by a ceramic under axial temperature gradient. In Proceedings of the International Heat Transfer Conference 13, Sydney, Australia, 13–18 August 2006. Volume RAD-10.
83. Delmas, A.; Robin-Carillon, L.; Oelhoffen, F.; Lanternier, T. Experimental and Theoretical Characterization of Emission from Ceramics at High Temperature: Investigation on Yttria-Stabilized Zirconia and Alumina. *Int. J. Thermophys.* **2010**, *31*, 1092–1110. [[CrossRef](#)]
84. Hay, B.; Hameury, J.; Fleurence, N.; Lacipiere, P.; Grelard, M.; Scoarnec, V.; Davee, G. New facilities for the measurements of high-temperature thermophysical properties at LNE. *Int. J. Thermophys.* **2014**, *35*, 1712–1724. [[CrossRef](#)]
85. Fu, T.; Duan, M.; Tang, J.; Shi, C. Measurements of the directional spectral emissivity based on a radiation heating source with alternating spectral distributions. *Int. J. Heat Mass Transf.* **2015**, *90*, 1207–1213. [[CrossRef](#)]
86. Manara, J.; Arduini-Schuster, M.; Keller, M. Infrared-optical characteristics of ceramics at elevated temperatures. *Infrared Phys. Technol.* **2011**, *54*, 395–402. [[CrossRef](#)]
87. Wang, B. The Study of Material's Spectral Emissivity Measurement System Based on FT-IR. Ph.D. Thesis, North China Electric Power University, Beijing, China, 2013.
88. Pierre, T.; Jiménez-Saelices, C.; Seantier, B.; Grohens, Y. Transient pulsed technique to characterize the radiative and conductive properties of bio aerogels. *Int. J. Therm. Sci.* **2017**, *116*, 63–72. [[CrossRef](#)]
89. Mendes, M.A.A.; Goetze, P.; Talukdar, P.; Werzner, E.; Demuth, C.; Rössger, P.; Wulf, R.; Gross, U.; Trimis, D.; Ray, S. Measurement and simplified numerical prediction of effective thermal conductivity of open-cell ceramic foams at high temperature. *Int. J. Heat Mass Transf.* **2016**, *102*, 396–406. [[CrossRef](#)]
90. Sans, M.; Schick, V.; Parent, G.; Farges, O. Experimental characterization of the coupled conductive and radiative heat transfer in ceramic foams with a flash method at high temperature. *Int. J. Heat Mass Transf.* **2020**, *148*, 119077. [[CrossRef](#)]
91. Fishedick, T.; Kind, M.; Dietrich, B. Radial two-phase thermal conductivity of ceramic sponges up to high temperatures—Experimental results and correlation. *Int. J. Therm. Sci.* **2017**, *114*, 98–113. [[CrossRef](#)]
92. Nicolau, V.P.; Raynaud, M.; Sacadura, J.F. Spectral radiative properties identification of fiber insulating materials. *Int. J. Heat Mass Transf.* **1994**, *37*, 311–324. [[CrossRef](#)]
93. Barreto, G.; Canhoto, P.; Collares-Pereira, M. Combined experimental and numerical determination of the asymmetry factor of scattering phase functions in porous volumetric solar receivers. *Sol. Energy Mater. Sol. Cells* **2020**, *206*, 110327. [[CrossRef](#)]
94. Randrianalisoa, J.; Baillis, D.; Pilon, L. Improved Inverse Method for Radiative Characteristics of Closed-Cell Absorbing Porous Media. *J. Thermophys. Heat Transf.* **2006**, *20*, 871–883. [[CrossRef](#)]
95. Loretz, M.; Coquard, R.; Baillis, D.; Maire, E. Metallic foams: Radiative properties/comparison between different models. *J. Quant. Spectrosc. Radiat. Transf.* **2008**, *109*, 16–27. [[CrossRef](#)]
96. Liu, M.; Ai, Q.; Yin, H.-C.; Xia, X.-L.; Tan, H.-P. Measurement model for near-infrared radiative properties of open-cell metallic foams based on transmittance spectra. *Int. J. Heat Mass Transf.* **2019**, *136*, 365–372. [[CrossRef](#)]
97. Tilioua, A.; Libessart, L.; Jeandel, G.; Lassue, S. Determination of radiative properties of polyester batting insulation material from hemispherical transmittance and reflectance measurements. *Appl. Therm. Eng.* **2016**, *105*, 594–604. [[CrossRef](#)]
98. Heisig, L.-M.; Markuske, K.; Werzner, E.; Wulf, R.; Fieback, T.M. Experimental and Simplified Predictive Determination of Extinction Coefficients of Ceramic Open-Cell Foams Used for Metal Melt Filtration. *Adv. Eng. Mater.* **2022**, *24*, 2100723. [[CrossRef](#)]
99. Doermann, D.; Sacadura, J.F. Heat Transfer in Open Cell Foam Insulation. *J. Heat Transf.* **1996**, *118*, 88–93. [[CrossRef](#)]

100. Dombrovsky, L.A.; Rousseau, B.; Echegut, P.; Randrianalisoa, J.H.; Baillis, D. High Temperature Infrared Properties of YSZ Electrolyte Ceramics for SOFCs: Experimental Determination and Theoretical Modeling. *J. Am. Ceram. Soc.* **2011**, *94*, 4310–4316. [[CrossRef](#)]
101. Guévelou, S.; Rousseau, B.; Domingues, G.; Vicente, J.; Caliot, C. Representative elementary volumes required to characterize the normal spectral emittance of silicon carbide foams used as volumetric solar absorbers. *Int. J. Heat Mass Transf.* **2016**, *93*, 118–129. [[CrossRef](#)]